Tricyclic SpiroLactams Kill Mycobacteria In Vitro and In Vivo by Inhibiting Type II NADH Dehydrogenases

Sushovan Dam, Salia Tangara, Claire Hamela, Theo Hattabi, Léo Faïon, Paul Carre, Rudy Antoine, Adrien Herledan, Florence Leroux, Catherine Piveteau, et al.

Tricyclic SpiroLactams Kill Mycobacteria *in vitro* and *in vivo* by Inhibiting Type II NADH Dehydrogenases

Sushovan Dam[1#], Salia Tangara[2#], Claire Hamela[3#,] Theo Hattabi[2], Léo Faïon[2], Paul Carre[1], Rudy Antoine[1], Adrien Herledan[2], Florence Leroux[2], Catherine Piveteau[2], Maxime Eveque[2], Marion Flipo[2], Benoit Deprez[2], Laurent Kremer[3,4], Nicolas Willand[2]*, Baptiste Villemagne[2]*, Ruben C. Hartkoorn[1]*

[#] Joint first authors: Sushovan Dam, Salia Tangara and Claire Hamela contributed equally

*Joint last and corresponding authors

[1] Univ. Lille, CNRS, Inserm, CHU Lille, Institut Pasteur Lille, U1019 - UMR 9017 - CIIL - Center for Infection and Immunity of Lille, F-59000 Lille, France.

[2] Univ. Lille, Inserm, Institut Pasteur de Lille, U1177 - Drugs and Molecules for Living Systems, F-59000, Lille, France.

[3] Centre National de la Recherche Scientifique, Institut de Recherche en Infectiologie de Montpellier, UMR 9004, Université de Montpellier, Montpellier, France.

[4] INSERM, IRIM, 34293 Montpellier, France.

ABSTRACT

It is critical that novel classes of anti-tuberculosis drugs are developed to combat the increasing burden of infections by multidrug resistant strains. To identify such a novel class of antibiotic, a chemical library of unique 3-D bioinspired molecules was explored revealing a promising, mycobacterium specific Tricyclic SpiroLactam (TriSLa) hit. Chemical optimization of the TriSLa scaffold delivered potent analogues with nanomolar activity against replicating and non-replicating *Mycobacterium tuberculosis*. Characterization of isolated TriSLa resistant mutants, and biochemical studies, found TriSLa to act as allosteric inhibitors of type II NADH dehydrogenases (Ndh-2 of the electron transport chain), resulting in an increase in bacterial NADH/NAD^+ ratios and decreased ATP levels. TriSLa are chemically distinct from other inhibitors of Ndh-2, but share a dependence for fatty acids for activity. Finally, *in vivo* proof of concept studies showed TriSLa to protect zebrafish larvae from *Mycobacterium marinum* infection, suggesting a vulnerability of Ndh-2 inhibition in mycobacterial infection.

INTRODUCTION

While global efforts to eradicate tuberculosis (TB) by improving drug access and treatment compliance have decreased deaths by 29 % over the last 2 decades, TB remains the leading cause of death by an infectious disease worldwide[1]. With a minimum of 6-months of multidrug therapy, current TB treatment is notoriously lengthy, a feature largely attributed to the difficulty of eliminating phenotypically drug-tolerant sub-populations of the causative bacteria *Mycobacterium tuberculosis (Mtb)* [2]. However, escalating infections by multidrug resistant (MDR) TB infections (483,000 cases of rifampicin-resistant TB reported in 2020 [1]) as well as extensively drug resistant (XDR) TB (12,350 cases reported in 2019 [3]) require even longer therapy with less efficient and tolerated second-line drugs. In recognition of this global health problem, the World Health Organisation (WHO) has placed TB at the highest critical global priority of antibiotic-resistant bacteria for the development of new antibiotics [4].

Concerted efforts to propose alternative and better antibiotics against drug-sensitive and -resistant TB have led to the approval of two novel classes of anti-TB drugs, the ATP synthase inhibitor bedaquiline [5], and the two nitroimidazole prodrugs, delamanid [6] and pretomanid [7]. Additional anti-TB molecules are at various levels of clinical and pre-clinical drug development that may feed our treatment options in the future [8–10]. Despite these increased efforts, it is clear that the TB drug development pipeline requires further supplementation with additional candidates, ideally acting on novel targets (to minimize cross-resistance) and impacting on drug-tolerant bacilli to shorten the duration of the treatment.

For the discovery of novel anti-TB drugs, phenotypic screening of chemical libraries on whole bacteria has proven to be the most successful approach [11]. The vast majority of synthetic molecules screened against *Mtb*, and hence emerged as leads, are largely flat (2-dimensional) in structure and comprise many sp^2-rich aromatic cores [12]. Such flat molecules are in stark contrast to the often complex 3-dimensional structures of natural products, historically representing an important source of antibiotics. The molecular shape of such biomolecules plays a key role in their interaction with protein targets [13]. Interestingly, the *Mtb* ATP synthase inhibitor bedaquiline buckles this trend as an antibiotic of synthetic origin, being highly 3D in shape, thanks to the two central adjacent highly substituted sp^3-hybridized carbon atoms. With the rational that molecules with increased 3D structures will allow for the probing of previously unexplored chemical and biological space, a "natural-like" chemical library with sp^3-rich synthetic molecules was assembled [14–19] and evaluated for anti-TB activity [20,21].

Herein, we show that the screening of chemical libraries with increased 3D diversity can result in the identification of novel chemical- and biological-space to combat *Mtb*. This work describes the identification of the Tricyclic SpiroLactam (TriSLa) chemical family and its chemical optimisation to

potent nanomolar anti-mycobacterial compounds with particular activity against *Mtb*. Target identification and validation studies revealed that TriSLa act through the inhibition of the mycobacterial type II NADH dehydrogenase. TriSLa exhibited a time-dependent bactericidal activity on *Mtb* and were also active on non-replicating and intracellular bacilli. Subsequent *in vivo* efficacy studies of TriSLa on *Mycobacterium marinum*-infected zebrafish larvae confirmed efficacy and validated type-2 NADH dehydrogenase as a vulnerable and druggable target in mycobacteria.

RESULTS

Discovery of Tricyclic SpiroLactam anti-tuberculosis lead compound

With the aim of investigating the anti-TB potential of new chemical spaces, we assembled a focused chemical library of 958 in-house synthetic "natural-like" compounds. These molecules display enhanced 3D properties, high number of sp^3-hybridized carbon atoms (≥ 12), a calculated molecular complexity greater than 0.76 [22] and a molecular shape index lower than 0.56, reflecting a greater sphericity (as measured using DataWarrior [23]) (**Figure S1a**). Screening of this chemical library at 10 µM on replicating *Mtb* strain H37Rv led to the identification of compounds **1** and **2** (**1**), two tricyclic spirolactams analogues that inhibited bacterial growth. Following *de novo* re-synthesis and purification of these hits, **1** and **2** were confirmed to have a minimal inhibitory concentration (MIC) against *Mtb* of 3.2 µM and 9.5 µM respectively (as measured using the resazurin reduction assay). The more potent analogue **1** is a small lead-like molecule (low molecular weight of 328 $g.mol^{-1}$, Lipinski and Veber compliant) with a high aqueous solubility (178 µM at pH 7.4) due to the basic nitrogen of the piperidine ring and favourable logD (2.7). The configuration of the stereogenic centres of **1** was confirmed by crystallization and X-ray diffraction of its hydrochloride salt **(Figure S1c**). To confirm the importance of the TriSLa configuration, compound **1**'s enantiomer (compound **3**, **Figure S1b**), was synthesized and found to be inactive against *Mtb* (MIC of 100 µM), supporting the hypothesis that the antibiotic activity is mediated by an interaction with a specific mycobacterial protein.

Hit-to-Lead optimization - Medicinal chemistry

Compound **1** represented an attractive starting point for the development of a new anti-TB chemotype, though its potency required improvement. Since replacement of the isopropyl moiety by a *sec*-butyl (compound **2**) was found to affect potency, we decided to explore other modifications in this position (

Table 1). Replacement of the isopropyl with smaller alkyl substituents (a methyl for compound **4** and an ethyl for compound **5**) led to a loss of activity (MIC > 100 µM and MIC = 18.8 µM, respectively). Similar result was obtained with a larger *tert*-butyl moiety (compound **6**, MIC = 25 µM). Introduction of a cyclopropyl (compound **7**, MIC = 37.5 µM) also led to a 1-log decrease in potency.

Table 1. Biological activities of compounds 1-7.

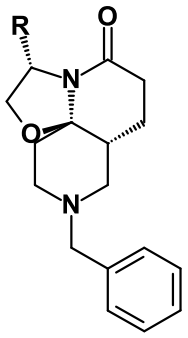

Compound	R	Anti-TB activity MIC_{98} (Range) (µM) [a]
1		3.2 (1.6-6.3)
2	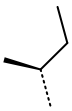	9.5 (6.3-12.5)
4		>100
5		18.8 (12.5-25)
6		25.0
7		37.5 (25-50)

[a] Anti-TB activity were determined on H37Rv grown in Middlebrook 7H9 media supplemented with 0.2 % glycerol, 0.05% tween 80 and 10% OADC. MIC_{98} represents the lowest concentration of compounds that prevented 98% of resazurin turnover by H37Rv compared to the untreated bacteria.

Overall, these SAR suggested that the isopropyl moiety of compound **1** cannot be advantageously replaced. In parallel, metabolic stability studies of compound **1** showed high clearance (**Table S1**) largely due to hydroxylation of the benzyl moiety (**Figure S2**). For these reasons, modifications of the benzyl group were next prioritized in an attempt to both metabolically stabilize compound **1** and increase its antimicrobial potency.

The introduction of electron-donating groups such as methyl (compound **8**, MIC = 1.7 µM) or methoxy (compound **9**, MIC = 4.7 µM) in position 4 of the phenyl ring did not impact antibacterial potency (**Table 2**). On the other hand, introduction of an electron-withdrawing chlorine atom (compound **10**, MIC = 0.25 µM) led to a marked (> 1-log) improvement in antibacterial potency. This effect was even

more pronounced using a trifluoromethyl (compound **11**, MIC = 0.10 µM) or trifluoromethoxy (compound **12**, MIC = 0.13 µM) moiety. Whilst the potency was improved, the hydrophobicity of **11** ($LogD_{7.4}$ = 3.9) and **12** ($LogD_{7.4}$ = 3.4) was increased, which had a slight impact on their solubility (148 and 133 µM, respectively). To address this, the phenyl group of **11** was replaced by a more polar pyridine group (compound **13**, $LogD_{7.4}$ = 2.7), which indeed led to an improved solubility (> 200 µM), but at the expense of anti-TB potency (MIC= 0.6 µM) (**Table 2**). As hypothesized, substitution of the phenyl ring prevented metabolism on this part of the molecule (**Figure S2**). However, microsomal stability remained only partially improved compared to compound **1**. Overall, these first structure-activity relationships study around compound **1** allowed for marked improvements to the TriSLa anti-TB potency.

Table 2. Summary of TriSLa anti-tuberculosis activity, biochemical Ndh-2 inhibition, and physicochemical properties.

Compound	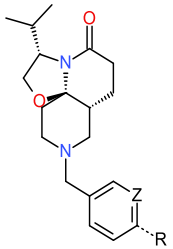 R	Z	Anti-TB activity MIC_{98} (Range) (µM) [a]	Inhibition of *Mtb* MBP-Ndh Mean IC_{50} ± SD (µM) n≥5 *E. coli* [b]	Inhibition of *Mtb* MBP-Ndh Mean IC_{50} ± SD (µM) n≥5 mc^2155 [c]	Inhibition of *Mtb* MBP-NdhA (from mc^2155) [c] Mean IC_{50} ± SD (µM) n≥5	Intra-cellular Mean IC_{50} ± SD (µM) [d]	Measured solubility in PBS (µM) [e]	PBS/Octanol partition coefficient $LogD_{7.4}$ [f]
1	-H	CH	3.2 (1.6-6.3)	0.34 ± 0.09	0.47 ± 0.12	0.98 ± 0.25	8.2 ± 1.6	178	2.7
8	$-CH_3$	CH	1.7 (0.75-2.5)	ND	ND	ND	ND	ND	ND
9	$-OCH_3$	CH	4.7 (2.5-6.3)	0.20 ± 0.12	0.89 ± 0.25	2.34 ± 0.29	ND	ND	ND
10	-Cl	CH	0.25 (0.16-0.31)	0.028 ± 0.011	0.042 ± 0.014	0.096 ± 0.026	ND	ND	ND
(11, BDM88689)	$-CF_3$	CH	0.10 (0.08-0.16)	0.012 ± 0.005	0.037 ± 0.025	0.059 ± 0.008	0.46 ± 0.11	148	3.4
(12, BDM88690)	$-OCF_3$	CH	0.13 (0.08-0.16)	0.012 ± 0.006	0.041 ± 0.017	0.057 ± 0.015	0.36 ± 0.03	133	3.9
(13, BDM89000)	$-CF_3$	N	0.59 (0.31-0.63)	0.032 ± 0.019	0.088 ± 0.027	0.33 ± 0.10	2.4 ± 1.3	>200	2.7

[a] Anti-TB activity were determined on H37Rv grown in Middlebrook 7H9 media supplemented with 0.2 % glycerol, 0.05% tween 80 and 10% OADC. MIC_{98} represents the lowest concentration of compounds that prevented 98% of resazurin turnover by H37Rv compared to the untreated bacteria. [b] Biochemical assays performed on recombinant MBP-Ndh purified from *E. coli*. [c] Biochemical assays performed on recombinant MBP-Ndh purified from *M. smegmatis* mc^2155. [d] Intracellular activity of compounds was investigated by determining the concentration that protected 50% of the macrophages (IC_{50}) from a lethal H37Rv infection (MOI 10), with macrophage viability determined using the resazurin reduction assay. [e] Solubility measured in PBS pH 7.4 starting from a 10 mM solution in DMSO of the compound. [f] LogD were measured at pH 7.4 between PBS and octanol. All compounds were tested at the same concentration (1 µM). n.d. not determined. MBP-Ndh stands for mannose binding protein tagged Ndh.

***In vitro* profiling of TriSLa activity**

Spectrum of TriSLa antibiotic activity. The spectrum of TriSLa antibiotic activity was next determined on a panel of mycobacteria as well as Gram-positive and -negative bacteria. Compounds **1**, **11** and **12** showed mycobacterium-specific activity with *Mtb*, *M. marinum* and *M. avium* being particularly susceptible (**Table 3**). Gram-positive and -negative bacteria were found to be resistant to TriSLa activity, including the efflux deficient *E. coli* Δ*tolC* (**Table 3**). These three TriSLa compounds showed no apparent cytotoxicity on BALB/3T3 cells at concentrations up to 100 µM.

Table 3. Spectrum of antibiotic activity of TriSLa inhibitors. MIC values (in µM) were determined using the resazurin reduction assay, except for *M. marinum* and *P. aeruginosa* where viability was determined visually. Data are presented as an average MIC of at least 3 independent biological replicates with the range of MICs (where there was a range) indicated in brackets.

Bacterial strain	MIC (µM)		
	Compound 1	**Compound 11**	**Compound 12**
M. tuberculosis (H37Rv)[#]	3.2 (1.6-6.3)	0.10 (0.08-0.16)	0.13 (0.08-0.16)
M. marinum (M strain)[#]	6.3	0.19 (0.16-0.31)	0.16
M. avium (TMC 724, ATCC-25291)[#]	13.1 (3.1-25)	0.55 (0.16-1.25)	0.38 (0.16-0.63)
M. smegmatis (mc^2155) [#]	29.2 (25-50)	1.3 (1.25-2.5)	1.3 (1.25-2.5)
M. abscessus (CIP104536, Smooth variant)[#]	≥ 100	5	8.1 (5-10)
M. abscessus (CIP104536, Rough variant)[#]	≥ 100	6.3 (5-10)	8.1 (5-10)
Bacillus subtillis (ATCC6633) ~	> 100	> 100	> 100
Staphylococcus aureus (SH1000) ~	> 100	> 100	> 100
Escherichia coli (BW25113) ~	> 100	> 100	> 100
Escherichia coli ΔtolC (BW25113 ΔtolC) ~	> 100	100	100
Pseudomonas aeruginosa (POA1) ~	> 100	> 100	> 100
Klebsiella pneumoniae (LMG 2095) ~	> 100	> 100	> 100
Acinetobacter baumannii (LMG-17978) ~	> 100	> 100	> 100

[#]Tested in Middlebrook 7H9 broth supplemented with 0.2% glycerol, 0.05% tween 80, and 10% OADC.
~Tested in Cation-adjusted Mueller Hinton II Broth (CAMHB).

Time-dependent bactericidal activity of TriSLa on replicating and non-replicating *M. tuberculosis.* To evaluate the bactericidal activity of TriSLa *in vitro*, the bacterial load (measured by colony forming units, cfu) was determined after 1 and 2 weeks of compound exposure at 1x, 2x and 4x MIC. Data revealed that 1x MIC of both **11** and **12** (150 nM) were bacteriostatic, while exposure to 2x and 4x MIC (300 and 600 nM) led to around a 0.8-log and 2.0 log drop in cfu after 1 and 2 weeks, respectively (**Figure 1a/b**). In line with previous reports [24], bedaquiline at 1x and 2x MIC (250 and 500 nM, respectively) was largely bacteriostatic over the 2 weeks exposure period (**Figure 1c**).

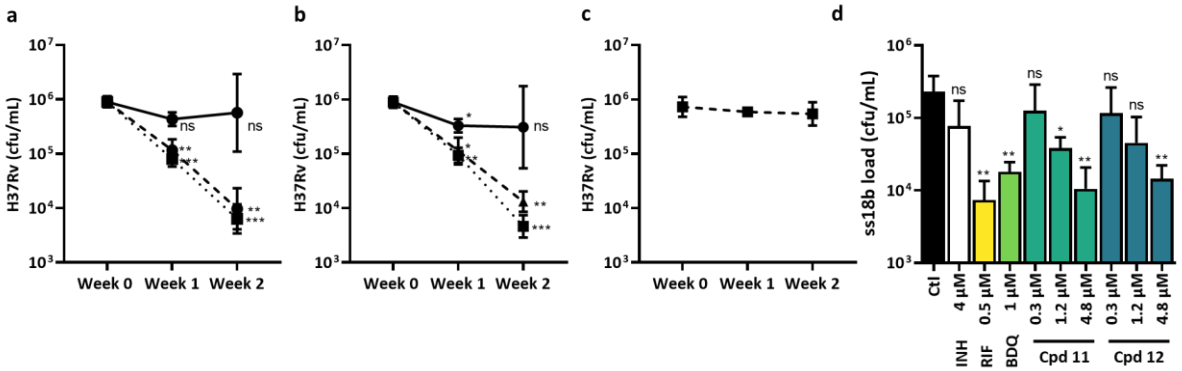

Figure 1. *In vitro* profile of TriSLa against replicating H37Rv (a-c) and non-replicating ss18b (d). The bactericidal activity of (a) **11**, (b) **12** and (c) bedaquiline was measured by cfu counting following 1 or 2 weeks of incubation with 1x MIC (filled circles, solid line), 2x MIC (filled triangles, dashed line) or 4x MIC (filled squares, dotted line). Data are mean and SEM of at least 3 independent biological replicates, and statistical analysis was performed with a paired t-test. (d) The bactericidal activity following 1-week incubation with TriSLA and control antibiotics (isoniazid (INH) bedaquiline (BDQ), rifampicin (RIF)) against non-replication ss18b-lux as measured by cfu counting. Data are mean and SEM of at least 3 independent biological replicates, and statistical test to compare compound exposure to no compound control was performed using a Two-tailed unpaired t test with Welch's correction. The time-dependent decrease in ss18b-lux luminescence is available in the **Figure S3**.

The activity of TriSLa compounds was then evaluated on non-replicating bacteria using a luciferase-expressing streptomycin starved 18b model of non-replicating *Mtb* (ss18b-lux [25]). By monitoring the ss18b-lux luminescence signal from the integrated *luxCDABE* reporter, a time-dependent decrease in luminescence was observed with rifampicin, bedaquiline and the TriSLa **11** and **12,** while isoniazid caused an increase in luminescence, as reported previously for cell wall inhibitors (**Figure S3**). This bactericidal activity was confirmed by plating of the remaining ss18b-lux bacteria following 7 days of antibiotic exposure on streptomycin containing plates and cfu counting. Data clearly show that exposure to high concentrations of isoniazid had no significant bactericidal activity against non-replicating ss18b-lux, while rifampicin and bedaquiline were bactericidal, as previously reported [25,26]. In this assay, both **11** and **12** showed a concentration-dependent killing of ss18b-lux, with

concentrations of 4.8 µM leading to a 1-2 log drop in bacterial counts, similar to that seen for 1 µM bedaquiline and 0.6 µM rifampicin (**Figure 1d**). While the potency of the **11** and **12** are lower than that observed on replicating bacteria.

TriSLa activity against intracellular *M. tuberculosis*. To define the activity of the TriSLa compounds against intracellular *Mtb*, their ability to protect differentiated THP-1 macrophages from a lethal infection dose of H37Rv was evaluated as a proxy to the number of intracellular bacteria. Data showed that control compounds isoniazid (IC_{50} = 204 ± 20 nM), rifampicin (IC_{50} = 91 ± 32 nM) and bedaquiline (IC_{50} = 34 ± 3 nM) were able to fully protect the macrophages from infection, in line with previously described data **(Figure S4)**. The TriSLa compounds tested were found to also protect macrophages from death by the intracellular infection in a similar hierarchy to that observed on extracellular H37Rv (**Table 2**), but protection was not absolute (did not achieve 100% protection) and required higher concentrations **(Figure S4**), suggesting that TriSLa are less effective on intracellular bacteria than isoniazid, rifampicin or bedaquiline.

Target identification of TriSLa

To gain insight into the mechanism of action of the TriSLa series, resistant *Mtb* mutants were isolated and characterised**.** After exposure to compound **1** at 14 and 28 µM**,** resistant H37Rv isolates were selected at a frequency of around 1 x 10^{-8} (6 and 4 colonies respectively, following the plating of 50 µL of OD_{600} = 50), with confirmation of resistance to **1** by REMA (MIC>100 µM). Whole genome sequencing and variant analysis of two resistant isolates found one (RC14.2) to carry a 97 bp base-pair deletion in the *ndhA* (Rv0392c) promoter (including a 17 bp truncation of the 5' end of neighbouring, non-essential *Rv0393* (encoding a 13E12 repeat family protein)) (**Figure S5**), and the other (RC28.2) to carry a non-synonymous single nucleotide polymorphism (SNP) in *ndh* (*Rv1854c*) leading to Tyr403Cys (**Table S2**) (sequences available at NCBI project number, PRJNA808942)**.** Similarly, validated **11-**resistant clones of H37Rv were isolated on 1 µM **11** at a frequency of resistance at around 3 x 10^{-7}, and Sanger sequencing of *ndh* and *ndhA* (including promoter) found them to carry an alternative non-synonymous mutation in the same *ndh* codon leading to Tyr403His and Tyr403Asn (**Table S2**). Finally, *M. marinum* isolates resistant to **11** were selected through sequential selection in liquid culture containing 4 µM TriSLa, followed by isolation of single clones on solid culture (direct selection on solid media led to high background). Sanger sequencing revealed these clones to similarly carry non-synonymous mutations in *ndh* (*MMAR_2728)*, but this time in conserved Gln334 codon, leading to Gln334Pro or Gln334Arg substitutions (**Table S2**).

Both *ndh* and *ndhA* encode for the two *Mtb* type II NADH dehydrogenases (Ndh-2, Ndh and NdhA) of the bacterial electron transport chain that mediate the transfer of electrons from NADH to menaquinone. Ndh and NdhA, share 67 % protein identity, with both Tyr403/Gln334 and surrounding amino acids conserved (**Figure S6**). In the absence of a protein structure of Ndh (or NdhA), structural models were generated by AlphaFold [27,28] and by homology (using SwissModel). Tyr403 and Gln334 were found in close proximity to each other (with a hydrogen bond interaction between their side chains according to AlphaFold) near the access pocket of menaquinone in the membrane-associated region of the protein (**Figure S7**). To date, mutations in this region of Ndh have not been associated with resistance to any antibiotic molecule. On the other hand, a deletion in the *ndhA* promoter (different to the one isolated here) that leads to an overexpression of *ndhA* has previously been isolated following selection to the 2-mercapto-quinazolinones family of Ndh-2 inhibitors [29]. In line with this, RT-qPCR found that the 97-base pair deletion found in the *ndhA* promoter of RC 14.2 had a 23-fold increased expression of *ndhA* relative to the parental strain, while expression of *ndh* remained unchanged (**Table S3**).

Biochemical inhibition of Ndh-2 by TriSLa

To confirm that TriSLa are Ndh-2 inhibitors, initial validation experiments focused Ndh, the primary NADH dehydrogenase in *Mtb* [30]. Using published methodology [29], recombinant maltose-binding protein (MBP) tagged Ndh (MBP-Ndh) was produced and purified from *E. coli* Rosetta cells, and confirmed to be active and reduce the surrogate electron acceptor menadione in the presence of NADH. Inhibition studies found that TriSLa were nanomolar inhibitors of NADH oxidation by MBP-Ndh (**Table 1**), and that this biochemical inhibition was in direct correlation with TriSLa MIC on *Mtb* (**Figure S8**). Biochemical evaluation of MBP-Ndh (Tyr403Cys) and MBP-Ndh (Gln334Pro) found these mutant proteins to be active, but 30-60 fold and 70-200 fold more resistant than MBP-Ndh to TriSLa-mediated inhibition, respectively (**Figure 2a, Table S4**). To determine if TriSLa also inhibit NdhA, a codon optimised MBP-NdhA was overexpressed and purified from *M. smegmatis* (recombinant MBP-NdhA purified from *E. coli* Rosetta was found to have poor catalytic activity), and inhibition studies found TriSLa to inhibit MBP-NdhA in a similar manner to MBP-Ndh (**Figure 2b**). Together these data validate TriSLa as pan-Ndh-2 inhibitors and confirm the importance of Tyr403 and Gln334 for TriSLa-mediated inhibition of Ndh.

TriSLa are non-competitive inhibitors of Ndh. As mentioned above, TriSLa resistance conferring mutations in Ndh (Tyr403 and Gln334) are located near the menaquinone-binding pocket of Ndh, suggesting that TriSLa could act as competitive inhibitors for menaquinone binding. Biochemical competition assays with varying concentrations of menadione (model electron acceptor) or NADH, however suggest TriSLa to not compete with either cofactor, and instead inhibit Ndh through a non-competitive or allosteric mechanism (**Figure 2c** and **d**).

Impact of TriSLa on the bacterial electron transport chain

As an inhibitor of Ndh-2, TriSLa were expected to impact the bacterial NADH/NAD^+ ratio and the functioning of the electron transport chain. To confirm this, NADH and NAD^+ concentrations were measured in *Mtb* following 2 and 24 hrs of exposure to 4x MIC concentrations of **11** or **12** (600 nM). Relative to untreated bacteria, TriSLa-exposed bacteria showed an increase in the NADH/NAD^+ ratio, driven by an increase in NADH and decrease in NAD^+ (**Figure 2e**). As previously published [24], exposure to bedaquiline also caused an increase in the NADH/NAD^+ ratio as a result from "back-pressure" on the electron transport chain, while rifampicin induced a decrease in NADH/NAD^+. TriSLa were also found to impact the electron transport chain as a whole, as exposure to **12** and **11 (Figure 2f)** caused a concentration dependent shutdown in bacterial ATP concentrations,

similar to that observed following exposure to bedaquiline **(Figure 2f).** Together these data support that inhibition of Ndh-2 in *Mtb* has a major impact on the bacterial electron transport chain leading to a decrease in ATP production.

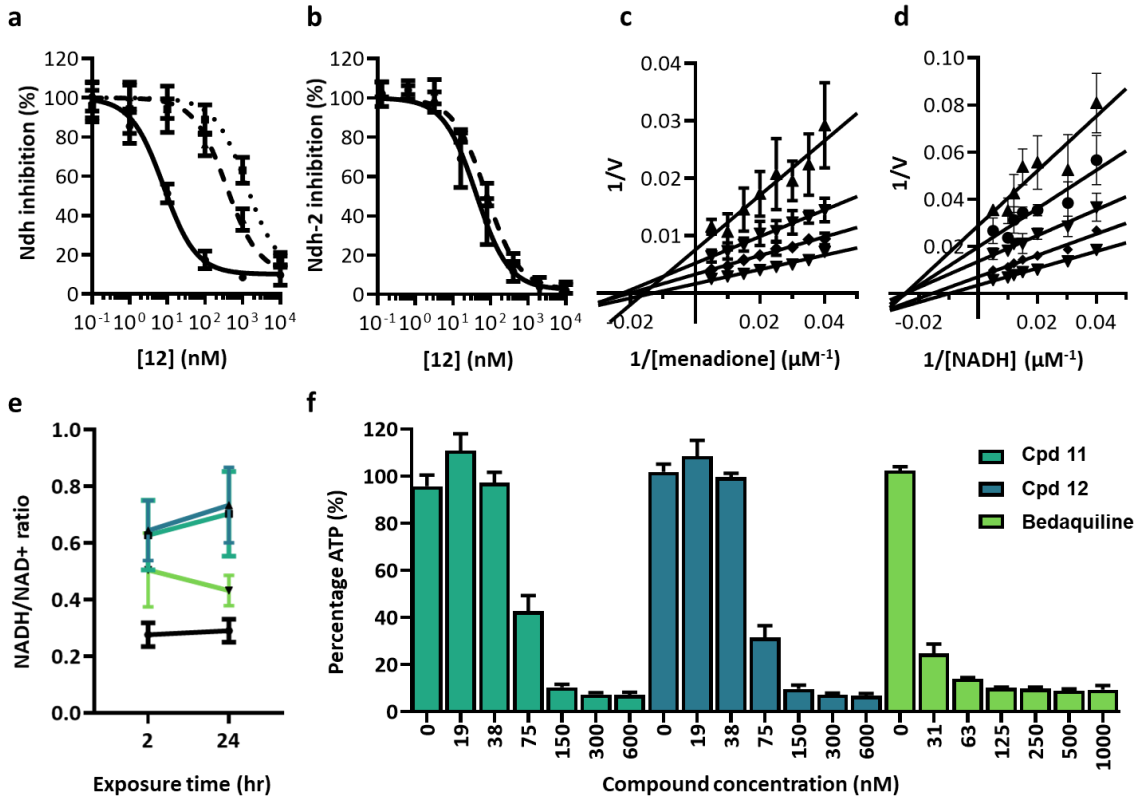

Figure 2: Biochemical target validation of TriSLa and impact on *Mtb* electron transport chain. (a) Compound **12** biochemical inhibition of NADH oxidation by recombinant *Mtb* MBP-Ndh (filled circles, solid line), MBP-Ndh(Y403C) (filled triangles, dashed line) and MBP-Ndh(Q334P) (filled squares, dotted line) overexpressed and purified using *E. coli*. Data are presented as a mean ± SD of at least 3 independent biological replicates **(b)** Compound **12** biochemical inhibition of NADH oxidation by recombinant *Mtb* MBP-Ndh (filled circles, solid line) and MBP-NdhA (filled triangles, dashed line) overexpressed and purified using *M. smegmatis*. **(c)** Lineweaver-Burk plot showing non-competitive inhibition of Ndh by **12** relative to menadione (n≥3), **(d)** Lineweaver–Burk plot showing non-competitive inhibition of Ndh by **12** relative to NADH (n≥3), **(e)** *Mtb* NADH/NAD^+ ratios measured following 2 and 24 hrs exposure to **11** (green-blue, 600 nM, 4x MIC), **12** (dark blue, 600 nM, 4x MIC) and bedaquiline (green, 1 µM, 4x MIC), compared to unexposed DMSO controls (black) (n≥3) **(f)** *Mtb* ATP concentrations measured following 24 hrs exposure to either **11** (green-blue), **12** (dark blue) and bedaquiline (green) (n≥3).

Impact of media composition on TriSLa antibiotic activity

Recent work has shown Ndh-2 to not be essential for *Mtb* growth in the absence of fatty acids, and that the removal of all fatty acids form the culture medium rendered Ndh-2 inhibitors such as 2-mercapto-quinazolinones inactive [31]. To verify this impact, the activity of TriSLa was re-evaluated in media lacking fatty acids (using fatty acid-free BSA) and data confirmed that the MIC of the compounds **1**, **11**, **12** and a control 2-mercapto-quinazolinones/ thioquinazoline (**CBR-5992**) all increased significantly, while no impact was observed for rifampicin or bedaquiline (**Table S5)**. To confirm that this impact is not *Mtb* specific, the role of fatty acids in the culture medium was also evaluated on *M. marinum*, confirming the same dependence of fatty acids for TriSLa activity (**Table S5**). Other published work showed that mutations in *ndh* of *M. smegmatis* and *M. bovis* BCG rendered these bacteria auxotrophic for serine [32], and that L-serine supplementation to the media rendered the Ndh-2 inhibitors (CBR-1825) less potent against *Mtb* in *vitro* [33]. In accordance with these results, supplementation of L-serine to the growth medium also caused a loss of antibiotic activity of the TriSLa compounds against H37Rv (**Table S6**). Finally, the impact of the detergents (Tween 80 or tyloxapol or neither) used in the culture media were not found to impact on TriSLa activity (**Table S6**).

***In vivo* efficacy on *M. marinum* infected zebrafish**

Considering the influence of media components on TriSLa antibiotic activity, it was considered a priority to evaluate the *in vivo* efficacy of TriSLa compounds. As the *in vitro* metabolic stability of the TriSLa compounds (**Table S1**) was too low for progression into murine efficacy studies of *Mtb* infection, it was decided to evaluate the *in vivo* efficacy of TriSLa on *M. marinum* infected zebrafish larvae, where compound exposure in the water is more stable. In such studies on acutely *M. marinum*-infected zebrafish larvae, the mycobacteria are phagocytosed by circulating macrophages and aggregate into foci that start to resemble granuloma [34–37]. Initial toxicity experiments confirmed that compounds **11**, **12** and **13** did not interfere with larval development or show any toxicity in non-infected zebrafish larvae (data not shown). Next, efficacy studies were performed as previously [34], where zebrafish larvae infected with *M. marinum* (expressing mWasabi) were exposed to different doses of TriSLa (refreshed daily) for a 4-days period (from 1 to 5 days post-infection (dpi)), followed by a 5-day period in the absence of antibiotics where survival was monitored (**Figure 3a**). Data confirmed that 4-day exposure compounds **11**, **12** and **13** significantly prolonged the survival of the infected zebrafish in a dose-dependent manner, starting from doses of 0.3, 0.3 and 1.2 µM (respectively), with higher doses of 4.8, 4.8 and 9.6 µM (respectively) prolonging survival by 3 days (**Figure 3b-d**). In complement, the bacterial load of the infected zebrafish was determined by fluorescence microscopy during the treatment phase of the study (at 2 and 4 days of exposure).

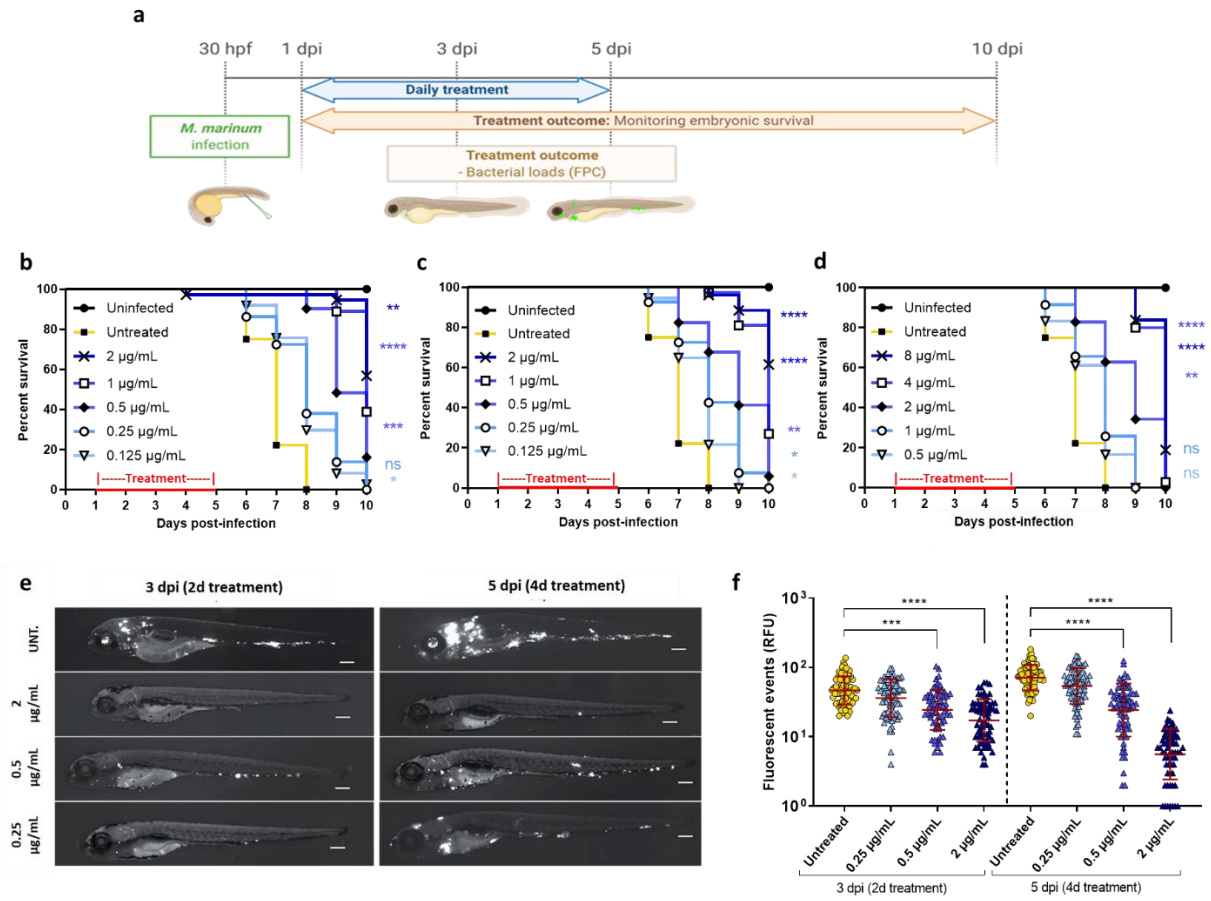

Figure 3: *In vivo* efficacy of TriSLa against *M. marinum*-infected embryonic zebrafish. (a) Schematic of the *in vivo* efficacy protocol showing the timeline of zebrafish embryo infection (200-250 colony-forming units (cfu) *M. marinum* expressing mWasabi), the exposure period to different concentrations of TriSLa (daily changes), and compound washout. hpf: hours post-fertilization; dpi: days post infection; FPC: Fluorescence pixel count. **(b-d)** Survival curve of *M. marinum*-infected zebrafish embryos monitored over the 10-day period post infection, with and without 4-day treatment of **(b)** Compound **11**, **(c)** Compound **12** and **(d)** compound **13**. Survival curves are the cumulative results of three experiments covering more than 25 infected zebrafish per group. Statistics to compare treatment groups were performed using the log rank (Mantel-Cox) statistical test (* $p < 0.05$, ** $P < 0.01$, **** $P < 0.0001$). **(e)** Representative sequential fluorescence images of *M. marinum* (mWasabi) infected zebrafish embryos following 2 or 4 days of treatment (3 and 5 dpi) with compound **12** at 0.25, 0.5 and 2 µg/mL, relative to untreated zebrafish (UNT.) Scale bar, 210 µm. (f) *M. marinum* infection burden in zebrafish embryo as quantified following 2 (3 dpi) and 4 (5 dpi) days of compound **12** exposure (0.25, 0.5 and 2 µg/ml) by pixel count (fluorescent events) using the ImageJ software. The data presented are the cumulative data of three independent experiment (each containing 20 to 25 embryos per group), with each data point representing one infected zebrafish larva. The error bar represents the mean and standard deviations of the cumulative dataset. Statistical comparison of the different groups was performed using a Mann-Whitney's t test, (*** $P < 0.001$, **** $P < 0.0001$).

Images of untreated infected larvae showed an intense dissemination of the *M. marinum* infection, with multiple large bacterial foci that increased over time (3 and 5 dpi) (**Figure 3e**), while 2 or 4-day treatment with 0.25 to 2 µg/mL (0.6 - 4.8 µM) of **12** clearly resulting in fewer and less intense infection foci (**Figure 3e**). Quantification of the bacterial load on a larger number of infected zebrafish (using fluorescence pixel count determination) showed that exposure to 0.5 µg/mL (1.2 µM) of **12** was bacteriostatic, preventing an increase in bacterial load from 2-4 days of exposure, while higher doses of 2 µg/mL (4.8 µM) lead to a significant decrease in the bacterial burden between 2 and 4 days of over the same period (**Figure 3f**). Together, these data confirm that inhibition of Ndh-2 has a significant impact on *M. marinum* infection in the zebrafish model of infection.

Chemistry

The unique rigid 3D Tricyclic SpiroLactam (TriSLa) core of the previously described molecules was obtained through stereoselective Meyers' lactamization.[17,38] This reaction uses readily accessible starting materials such as ketoesters (or ketoacids) as bi-electrophile and alkanolamines as bi-nucleophile to generate complex fused ring systems. Lactams **1-7** were obtained by reacting methyl 3-(1-benzyl-4-oxo-3-piperidyl)propanoate (obtained by esterification of its acid analogue, previously synthesized according to literature)[17] with the appropriate β-amino alcohol (**Scheme 1**) in yields ranging from 27 to 75% . Only partial stereoselectivity was observed with mildly hindered β-amino alcohol (compounds **4** and **5**), while only one stereoisomer was obtained with highly hindered β-amino alcohol (compounds **1**, **2**, **6** and **7**).

Scheme 1: Synthesis of analogs 1-7[(a)]

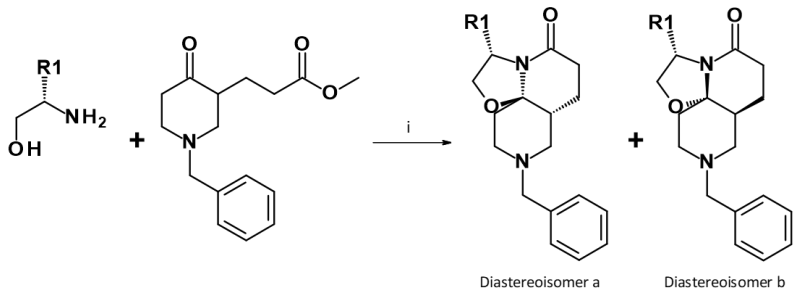

compound	R1	Yield (%)	a/b
1	isopropyl	75	100/0
2	s-btuyl	45	100/0
4	methyl	46	70/30
5	ethyl	73	70/30
6	cyclopropyl	27	100/0
7	t-butyl	40	100/0

[(a)] Reagents and conditions: (i) methyl 3-(1-benzyl-4-oxo-3-piperidyl)propanoate (1 eq), amino-alcohol (1.2–3 eq), pivalic acid (1.2–3 eq), Toluene, 150 °C (thermic for 20 h or microwave irradiations for 1-4 h).

Analogues **8**-**13** were synthesized from compound **1** (**Scheme 2**), through N-debenzylation using Pd/C and ammonium formate followed by N-alkylation using nucleophilic substitutions (compounds **8**-**12**) or reductive amination (compound **13**).

Scheme 2: Synthesis of analogs 8-13[(a)]

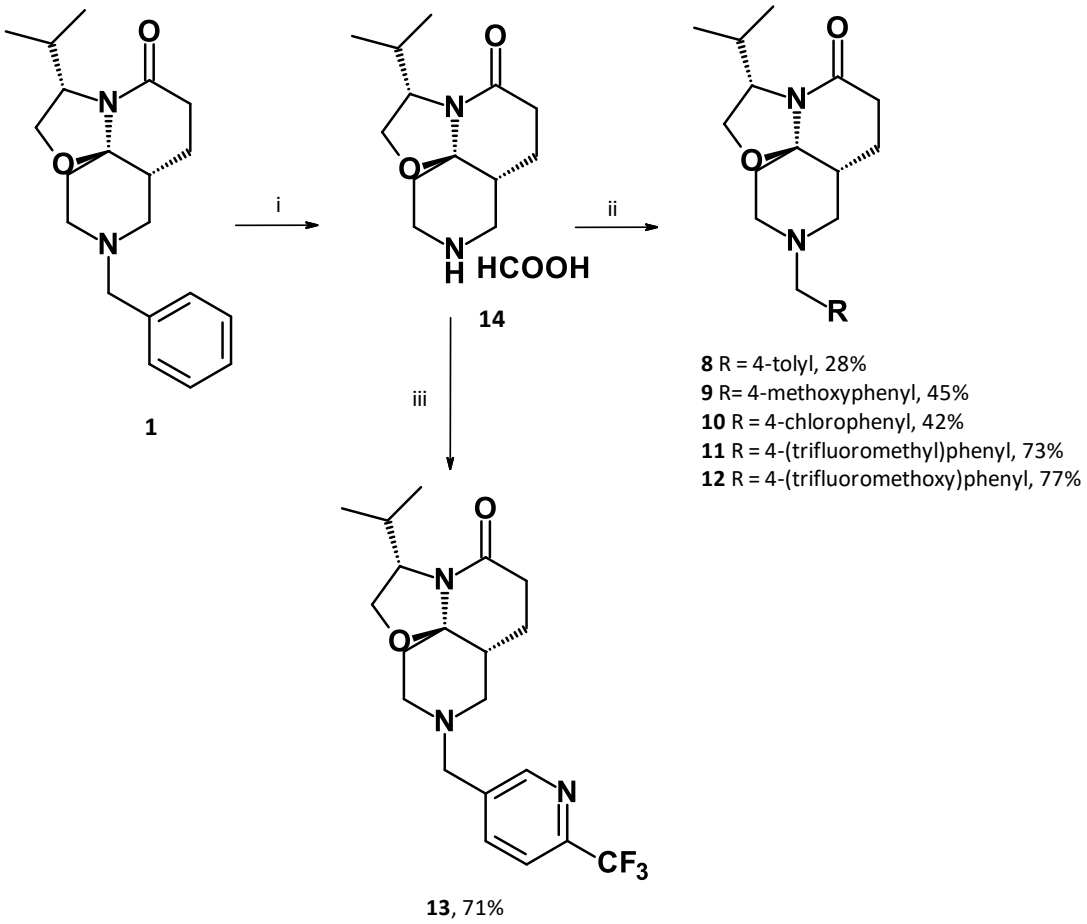

8 R = 4-tolyl, 28%
9 R= 4-methoxyphenyl, 45%
10 R = 4-chlorophenyl, 42%
11 R = 4-(trifluoromethyl)phenyl, 73%
12 R = 4-(trifluoromethoxy)phenyl, 77%

13, 71%

[(a)] Reagents and conditions: (i) Pd/C 10 % (10 mol%), HCO_2H (5 eq), reflux, 30 min; (ii) 14 (1 eq), K_2CO_3 (3 eq), RCH_2Br (1–1.5 eq), NaI (0–1 eq), MeCN, RT, 1–20 h; (iii) **14** (1 eq), 6-(trifluoromethyl)pyridine-3-carbaldehyde (3.6 eq), $Ti(OiPr)_4$ (1.8 eq), $NaBH(OAc)_3$ (3.6 eq), dichloroethane, RT, overnight.

DISCUSSION

Natural products and their hemisynthetic derivatives are a rich source of bioactive molecules and make up the bulk of the antibiotic classes currently used. Natural products often boast an increased chemical complexity [39,40], particularly emphasized by an abundance of chiral tetrahedral carbons. This increased 3D aspect allows natural products to occupy a different biological space compared to flatter

molecules found in many drug-like screening collections. In this work, we demonstrate that screening synthetic focused chemical libraries enriched with nature-inspired scaffolds is a promising approach to identify novel anti-tuberculosis chemical scaffolds with potent activity.

In recent years, a number of anti-tuberculosis molecules targeting Ndh-2 have been described, including 2-mercapto-quinazolinones [29,33], quinolones [41,42] and quinolinyl-pyrimidines [43,44], though no *in* vivo efficacy studies have been conducted thus far for these inhibitors. Overall these inhibitors share similar structural features, being largely planar (large number of sp^2-hybridized atoms) and carrying a central bicyclic aromatic ring, in sharp contrast to the highly 3D (large number of sp^3-hybridized atoms) structure of the TriSLa compounds described here. Despite these structural differences, TriSLa do share common attributes with the most potent of these compounds, (2-mercapto-quinazolinones [29,33]). This includes comparable potency, being pan Ndh-2 inhibitors, being non-competitive inhibitors of Ndh, displaying activity modulated by promoter mutation in *ndhA*, by L-serine and by fatty acid content in the media. By having structurally diverse chemical scaffolds targeting a protein is particularly worthwhile in drug development as this allows for different ADME/Tox profile and provides an alternative in case of drug development flags such as toxicity, pharmacokinetics (including tissue distribution), and off-target effects that are more often associated to the chemical scaffold. Together this will help increase the chance of Ndh-2 inhibitors to enter clinical development. In this study, we report point mutations in Ndh that confer resistance to TriSLa, suggesting that these inhibitors act specifically at the Ndh-2 protein-membrane interface. Multiple protein alignment of Ndh-2 orthologues from a panel of bacteria show Gln344 to be highly conserved between bacteria, while Tyr403 is conserved amongst mycobacteria, which likely explains their mycobacteria-specific antibacterial spectrum. Ndh structure models computed using Alphafold [27,28] interestingly place the side chains of Tyr403 and Gln334 in close proximity to each other with possible hydrogen bonding interactions between their side chains. These residues are likely flexible, but in the model these interacting residues appears to greatly limit the size of the menaquinone access pocket (**Figure S8**). A hypothesis on the mechanism of Ndh-2 inhibition by TriSLa, is that they bind and stabilise this closed confirmation and hence prevent the access of menaquinone, thus preventing its subsequent reduction. However, future structural biology efforts are needed to further elucidate how these two potent inhibitors are acting on Ndh-2.

Recent work demonstrated that *Mtb* could survive *in vitro* without either of its *ndh-2* genes when grown in the absence of exogenous fatty acids [31], and that this double *ndh-2* deleted strain could still infect mice, though it was partially attenuated with a 26-fold lower maximal titre [31]. As demonstrated

for 2-mercapto-quinazolinones Ndh-2 inhibitors [31], the removal of all fatty acids from the media, or additional serine supplementation (greater than natural available concentration) also prevent the activity of TriSLa *in vitro*, confirming the vulnerability of Ndh-2 in the presence of fatty acids. Together, this work called into question the potential of Ndh-2 inhibitors in the fight against tuberculosis infections, and reasons that efficacy will depend on the fatty acid content of the compartments in which the mycobacteria reside. Data presented here highlight that despite TriSLa activity on *M. marinum* also being dependent on fatty acids, TriSLa treatment of *M. marinum*- infected zebrafish did result in concentration-dependent efficacy, both prolonging zebrafish survival and decreasing bacterial loads. This therefore evokes that, at least in this infection model, a significant proportion of *M. marinum* is likely to reside in a fatty acid-containing compartment, such as granuloma type structures, which are considered fatty acid rich. Indeed, recent work has shown that the zebrafish/*M. marinum* granuloma contains the lipid-rich foam cells and that this differentiation of macrophages into foam cells is stimulated by the mycobacterial ESX-1 type VII secretion locus [45].

This observed efficacy is, however, in contrast to the aforementioned finding that despite partial attenuation, Ndh-2 double knockout *Mtb* strains could still grow in C57BL/6 mice [31]. Apart from possible differences in Ndh-2 vulnerability in *Mtb* and *M. marinum*, differences in the bacterial compartmental distribution (such as granulomas, intracellular, extracellular) and its associated fatty acid content may also be a factor to consider. In *Mtb*-infected C57BL/6 mice the infection is largely believed to reside within macrophages, where the primary carbon source is expected to be cholesterol (depending on the macrophage) and where fatty acid availability is likely lower than in granulomas. TriSLa (and 2-mercaptoquinoxalines) are poorly active against these intracellular infections and may hence contribute to this difference. As granuloma are believed to play a major role in human *Mtb* infections, more work is needed to define the exact vulnerability of Ndh-2, and the potential of Ndh-2 inhibitors as anti-tuberculosis agent, alone and in combination in animal models where granuloma formation is observed. For that purpose, further efforts will all focus on generating TriSLa compounds with an optimal pharmacokinetic profile.

Together, this work presents a new anti-mycobacterial chemical scaffold that acts through allosteric inhibition of Ndh-2. *In vitro* profiling of the TriSLa show them to have a time-dependant bactericidal activity on replicating and non-replicating bacteria, and *in vivo* efficacy studies confirm the vulnerability of this protein in *M. marinum* infected zebrafish. Future medicinal chemistry will aim to confirm Ndh-2 vulnerability for *Mtb* in various murine models of infection, and define TriSLa based treatment regimens.

EXPERIMENTAL SECTION

Chemical synthesis. *General information.* All reagent-grade chemicals and anhydrous solvents for synthesis, analysis and purification, were obtained from commercial suppliers and were used as received without further purification.

Flash chromatography was performed using a Puriflash PF-430 with silica gel cartridges (Buchi silica 40 µm). ELSD and UV detection (254 nm) were used to collect the desired product. Reverse flash chromatography was performed using a CombiFlash® Rf200 with C18 cartridges (Buchi C18 40 µm). UV detection (215 and 254 nm) was used to collect the desired product.

^{1}H NMR and ^{13}C NMR spectra were recorded on a Bruker DRX-300 spectrometer. Chemical shifts (δ) are in parts per million (ppm). The ^{1}H spectra were calibrated to signals from CD_2Cl_2 (δ 5.36 ppm) or $CDCl_3$ (δ 7.26 ppm), and ^{13}C spectra from CD_2Cl_2 (δ 53.5 ppm) or $CDCl_3$ (δ 77.16 ppm). ^{1}H NMR spectra are reported as following: chemical shift (ppm), multiplicity (s: singlet; brs: broad singlet; d: doublet; dd: doublet of doublet; t: triplet; td: triplet of doublet; m: multiplet), coupling constants in Hertz (Hz) and integration. Proton and carbon signal assignments were established using COSY, HSQC-DEPT and HMBC spectra.

LC-MS Waters system was equipped with a 2747 sample manager, a 2695 separation module, a 2996 photodiode array detector (200-400 nm) and a Micromass ZQ2000 detector (scan 100-800). XBridge C18 column (50 mm x 4.6 mm, 3.5µm, Waters) was used. The injection volume was 20 µL. A mixture of water and acetonitrile was used as mobile phase in gradient-elution. The pH of the mobile phase was adjusted with HCOOH and NH_4OH to form a buffer solution at pH 3.8. The analysis time was 5 min (at a flow rate at 2 mL/min), 10 min (at a flow rate at 1 mL/min) or 30 min (at a flow rate at 1 mL/min). Purity (%) was determined by reversed phase HPLC, using UV detection (215 nm). All final compounds showed purity greater than 95%.

High-resolution mass spectra (HRMS) analysis was performed on a LC-MS system equipped with a LCT Premier XE mass spectrometer (Waters), using a XBridge C18 column (50 mm x 4.6 mm, 3.5µm, Waters). A gradient starting from 98% H2O 5 mM Ammonium Formate pH 3.8 and reaching 100% MeCN 5 mM Ammonium formate pH 3.8 within 3 min at a flow rate of 1 mL was used.

Methyl-3-(1-benzyl-4-oxo-3-piperidyl)propanoate. To a solution of 3-(1-benzyl-4-oxo-3-piperidyl)propanoic acid (19.3 g, 73.9 mmol) in methanol (200 mL), was added $SOCl_2$ (5.9 mL, 81.3 mmol) dropwise at room temperature. The mixture was then stirred at 55 °C for 1 h. The solvent was removed under vaccum and the mixture was dissolved in 0.1 N HCl (100 mL), and stirred at room temperature for 1 h. A saturated aqueous solution of Na_2CO_3 was added until pH 10. The solution was extracted with ethyl acetate. The organic layer was dried over $MgSO_4$, and the solvent was removed under reduced pressure to give the crude product, which was purified by silica gel chromatography (cyclohexane/ethyl acetate: 7/3 to 0/10) to afford Methyl 3-(1-benzyl-4-oxo-3-piperidyl)propanoate (6.73 g, 33%), as a colorless oil. ^{1}H NMR (300 MHz, CD_2Cl_2): δ 7.36-7.25 (m, 5H), 3.64 (d, *J* = 13.1 Hz, 1H), 3.61 (s, 3H), 3.57 (d, *J* = 13.1 Hz, 1H), 3.08-2.97 (m, 2H), 2.62-2.11 (m, 7H), 2.08-1.95 (m, 1H), 1.53-1.42 (m, 1H) ppm. [ES+ MS] m/z 276 (MH+). ^{1}H NMR data matched those reported previously (Idzik, T. J.; Myk, Z. M.; Peruzynska, M.; Maciejewska, G.; Drozdzik, M.; Sosnicki, J. G. Arylation of enelactams using TIPSOTf: reaction scope and mechanistic insight. *Org. Chem. Front.* **2021**, *8*, 708-720).

General protocol 1: Diastereoselective Meyers' lactamization

A solution of pivalic acid (1.2-3 eq) in toluene (0.2N) was added to methyl 3-(1-benzyl-4-oxo-3-piperidyl) propanoate (1 eq). The appropriate amino-alcohol (1.2-3 eq) was added (when the amine is used as a chlorohydrate, DIEA (1.2-3 eq) was added). The mixture was refluxed at 150 °C (thermic for 20 h or microwave irradiations for 1−4h). When the conversion of the keto-ester was judged complete by LC/MS, the solution was dissolved in H_2O, extracted with ethyl acetate or dichloromethane. The layers were separated. The organic layer was dried over $MgSO_4$, filtered and concentrated under vacuum to give the crude product, which was purified, to afford the corresponding desired product.

(3S,7aR,11aR)-9-benzyl-3-isopropyl-2,3,6,7,7a,8,10,11-octahydrooxazolo[2,3-j][1,6]naphthyridin-5-one **(1).** The product **1** was obtained from L-valinol using general protocol 1. The crude product was purified by flash chromatography column over silica (cyclohexane/ethyl acetate: 1/0 to 6/4) to afford the desired product **1** (Yield = 75%, white powder) as a single diastereoisomer. **^{1}H NMR** (300 MHz, $CDCl_3$): δ 7.33-7.20 (m, 5H, ^{Ar}CH), 4.13-4.03 (m, 1H, ^{3}CH), 3.98 (dd, *J* = 8.6, 7.6 Hz, 1H, ^{2}CH$_2$), 3.77 (dd, *J* = 8.6, 6.2 Hz, 1H, ^{2}CH$_2$), 3.54 (d of AB system, *J* = 13.3 Hz, 1H, ^{12}CH$_2$), 3.41 (d of AB system, *J* = 13.1 Hz, 1H, ^{12}CH$_2$), 2.77-2.64 (m, 2H, ^{10}CH$_2$ and ^{8}CH$_2$), 2.62-2.51 (m, 1H, ^{6}CH$_2$), 2.49-2.29 (m, 3H, ^{8}CH$_2$, ^{7}CH$_2$ and ^{6}CH$_2$), 2.25-2.16 (m, 1H, ^{10}CH$_2$), 2.09-1.89 (m, 2H, ^{13}CH and ^{11}CH$_2$), 1.83-1.73 (m, 1H, ^{11}CH$_2$), 1.72-1.55 (m, 2H, ^{7a}CH, and ^{7}CH$_2$), 0.94 (d, *J* = 6.8 Hz, 3H, $^{14 \text{ or } 15}$CH$_3$), 0.90 (d, *J* = 6.8 Hz, 3H, $^{14 \text{ or } 15}$CH$_3$) ppm. **^{13}C NMR** (75 MHz, $CDCl_3$): δ 170.2 (^{5}CO), 138.9 (^{Ar}Cq), 128.7, 128.3, 127.0 (^{Ar}CH), 92.7 (^{11a}Cq), 66.2 (^{2}CH$_2$), 62.5 (^{12}CH$_2$), 61.2 (^{3}CH), 54.8 (^{8}CH$_2$), 50.7 (^{10}CH$_2$), 40.4 (^{7a}CH), 32.4 (^{13}CH), 32.4 (^{11}CH$_2$), 30.8 (^{6}CH$_2$), 21.9 (^{7}CH$_2$), 19.9 ($^{14 \text{ or } 15}$CH$_3$), 18.7 ($^{14 \text{ or } 15}$CH$_3$) ppm. **HRMS (ESI,m/z)**: $[M+H]^+$ calcd. for

$C_{20}H_{29}N_2O_2$, 329.2229; found 329.2227.

*(3S,7aR,11aR)-9-benzyl-3-[(1S)-1-methylpropyl]-2,3,6,7,7a,8,10,11-octahydrooxazolo[2,3-j][1,6]naphthyridin-5-one **(2)**.*The product **2** was obtained from (2S,3S)-2-amino-3-methyl-pentan-1-ol using general protocol 1. The crude product which was purified by preparative HPLC using MeCN +0.1%HCOOH and H_2O + 0.1%HCOOH gradient (9/1 to 0/10) to afford the product **2** (Yield = 45%, yellow oil) as a single diastereoisomer. **^{1}H NMR** (500 MHz, $CDCl_3$): δ 7.39-7.21 (m, 5H, ^{Ar}CH), 4.14 (dd, *J* = 7.5, 7.3 Hz, 1H, ^{3}CH), 3.97 (dd, *J* = 8.8, 7.5 Hz, 1H, ^{2}CH$_2$), 3.75 (dd, 1H, *J* = 8.8, 6.9 Hz, 1H, ^{2}CH$_2$), 3.65-3.38 (m, 2H, ^{12}CH$_2$), 2.76-2.20 (m, 7H, ^{10}CH$_2$, ^{8}CH$_2$, ^{7}CH$_2$, and ^{6}CH$_2$), 1.89-1.54 (m, 5H, ^{13}CH, ^{11}CH$_2$, ^{7}CH$_2$, and ^{7a}CH), 1.49-1.38 (m, 1H, ^{15}CH$_2$), 1.19-1.05 (m, 1H, ^{15}CH$_2$), 0.89 (t, *J* = 7.4 Hz, 3H, ^{16}CH$_3$), 0.85 (d, *J* = 6.8 Hz, 3H, ^{14}CH$_3$) ppm. **^{13}C NMR** (125 MHz, $CDCl_3$): δ 170.3 (^{5}CO), 138.7 (^{Ar}Cq), 128.9, 128.5, 127.1 (^{Ar}CH), 92.2 (^{11a}Cq), 65.8 (^{2}CH$_2$), 62.5 (^{12}CH$_2$), 60.8 (^{3}CH), 54.7 (^{10}CH$_2$), 50.7 (^{8}CH$_2$), 40.4 (^{7a}CH), 38.2 (^{13}CH), 32.0 (^{11}CH$_2$), 30.8 (^{6}CH$_2$), 27.2 (^{15}CH$_2$), 21.9 (^{7}CH$_2$), 14.9 (^{14}CH$_3$), 12.0 (^{16}CH$_3$) ppm. **HRMS (ESI,m/z)**: $[M+H]^+$ calcd. for $C_{21}H_{31}N_2O_2$, 343.2386; found: 343.2382.

(3R,7aS,11aS)-9-benzyl-3-isopropyl-2,3,6,7,7a,8,10,11-octahydrooxazolo[2,3-j][1,6]naphthyridin-5-one **(3).** The product **3** was obtained from (2R)-2-amino-3-methyl-butan-1-ol using general protocol 1. The crude product was purified by flash chromatography column over silica (cyclohexane/ethyl acetate: 1/0 to 6/4) to afford the desired product **3** (Yield = 61%, colorless oil) as a single diastereoisomer. The datas obtained (NMR and HRMS) were the same as the data described for his enantiomer compound **1**.

(3S,7aR,11aR)-9-benzyl-3-methyl-2,3,6,7,7a,8,10,11-octahydrooxazolo[2,3-j][1,6]naphthyridin-5-one **(4a)** *and (3S,7aS,11aS)-9-benzyl-3-methyl-2,3,6,7,7a,8,10,11-octahydrooxazolo[2,3-j][1,6]naphthyridin-5-one* **(4b)**. The products **4a** and **4b** were obtained from (2S)-2-aminopropan-1-ol using general protocol 1. The crude product was purified by preparative HPLC using MeCN +0.1%HCOOH and H_2O + 0.1%HCOOH gradient (9/1 to 0/10). A basification and an extraction at 10 pH with a saturated solution of Na_2CO_3 were carried out on the recovered fraction and the combined organic layers were dried over $MgSO_4$. The solvent was removed under reduced pressure the desired to afford products **4a** and **4b** (Yield = 46%, yellow oil), as a mixture of two diastereoisomers (d.r.(4a/4b) = 7/3). Data for the major diastereoisomer **4a**: **^{1}H NMR** (300 MHz, CD_2Cl_2) : δ 7.38-7.20 (m, 5H, ^{Ar}CH), 4.28-4.06 (m, 2H, ^{3}CH and ^{2}CH$_2$), 3.62 (dd, *J* = 13.0 Hz, *J* = 1.3 Hz, 1H, ^{2}CH$_2$), 3.53 (d, *J* = 13.4 Hz, 1H, ^{12}CH$_2$), 3.42 (d, *J* = 13.4 Hz, 1H, ^{12}CH$_2$), 2.78-2.63 (m, 2H, ^{10}CH$_2$ and ^{8}CH$_2$), 2.58-2.15 (m, 5H, ^{10}CH$_2$, ^{8}CH$_2$, ^{7}CH$_2$ and ^{6}CH$_2$), 1.99-1.60 (m, 5H, ^{11}CH$_2$, ^{7}CH$_2$ and ^{7a}CH), 1.29 (d, *J* = 6.1 Hz, 3H, ^{13}CH$_3$) ppm. **^{13}C NMR** (75 MHz, CD_2Cl_2): δ 168.9 (^{5}CO), 139.4 (^{Ar}Cq), 129.0, 128.5, 127.3 (^{Ar}CH), 92.6 (^{11a}Cq), 69.7 (^{2}CH$_2$), 62.7

($^{12}CH_2$), 55.2 ($^{8}CH_2$), 51.7 (^{3}CH), 50.9 ($^{10}CH_2$), 40.7 (^{7a}CH), 31.6 ($^{11}CH_2$), 31.1 ($^{6}CH_2$), 22.9 ($^{7}CH_2$), 20.2 ($^{13}CH_3$) ppm. **HRMS (ESI, m/z)**: $[M+H]^+$ calcd. for $C_{18}H_{25}N_2O_2$, 301.1916; found: 301.1914.

(3S,7aR,11aR)-9-benzyl-3-ethyl-2,3,6,7,7a,8,10,11-octahydrooxazolo[2,3-j][1,6]naphthyridin-5-one **(5a) a***nd (3S,7aR,11aR)-9-benzyl-3-ethyl-2,3,6,7,7a,8,10,11-octahydrooxazolo[2,3-j][1,6]naphthyridin-5-one* **(5b).** The products **5a** and **5b** were obtained from (2S)-2-aminobutan-1-ol using general protocol 1. The crude product was purified by preparative HPLC using MeCN +0.1%HCOOH and H_2O + 0.1%HCOOH gradient (9/1 to 0/10) to afford products **5a** and **5b** (Yield = 73%, yellow oil), as mixture of two diastereoisomers (d.r.(5a/5b) = 7/3). Data for the major diastereoisomer **5a**: **^{1}H NMR** (300 MHz, CD_2Cl_2) : δ 7.42-7.28 (m, 5H, ^{Ar}CH), 4.23-4.04 (m, 2H, ^{3}CH and $^{2}CH_2$), 3.76-3.66 (m, 1H, $^{2}CH_2$), 3.73 (d, *J* = 13.3 Hz, 1H, $^{12}CH_2$), 3.59 (d, *J* = 13.3 Hz, 1H, $^{12}CH_2$), 2.97-2.75 (m, 2H, $^{10}CH_2$ and $^{8}CH_2$), 2.58-2.15 (m, 5H, $^{10}CH_2$, $^{8}CH_2$, $^{7}CH_2$ and $^{6}CH_2$), 2.09-1.67 (m, 5H, $^{13}CH_2$, $^{11}CH_2$, $^{7}CH_2$ and ^{7a}CH), 1.50-1.34 (m, 1H, $^{13}CH_2$), 0.92 (t, *J* = 7.5 Hz, 3H, $^{14}CH_3$) ppm. **^{13}C NMR** (75 MHz, CD_2Cl_2): δ 169.0 (^{5}CO), 136.7 (^{Ar}Cq), 129.3, 128.3, 127.5 (^{Ar}CH), 91.6 (^{11a}Cq), 70.0 ($^{2}CH_2$), 61.9 ($^{12}CH_2$), 57.0 (^{3}CH), 54.1 ($^{8}CH_2$), 50.0 ($^{10}CH_2$), 39.9 (^{7a}CH), 30.6 ($^{11}CH_2$), 30.6 ($^{6}CH_2$), 27.8 ($^{13}CH_2$), 22.1 ($^{7}CH_2$), 10.2 ($^{14}CH_3$) ppm. **HRMS (ESI, m/z)**: $[M+H]^+$ calcd. for $C_{19}H_{27}N_2O_2$, 351.2017; found: 351.2093.

(3S,7aR,11aR)-9-benzyl-3-cyclopropyl-2,3,6,7,7a,8,10,11-octahydrooxazolo[2,3-j][1,6]naphthyridin-5-one **(6)**. The product **6** was obtained from (2S)-2-amino-2-cyclopropyl-ethanol;hydrochloride using general protocol 1. The crude was purified by preparative HPLC using H_2O + 0.1% HCOOH/MeCN + 0.1% HCOOH (90/10 to 0/100) to afford the desired product **6** (Yield = 27%, brown oil), as a single diastereoisomer. **^{1}H NMR** (300 MHz, $CDCl_3$): δ 7.36-7.23 (m, 5H, ^{Ar}CH), 4.15 (dd, *J* = 8.5 Hz, *J* = 8.4 Hz, 1H, $^{2}CH_2$), 3.86 (dd, *J* = 8.9=5 Hz, *J* = 6.8 Hz, 1H, $^{2}CH_2$), 3.75-3.62 (m, 1H, ^{3}CH), 3.58 (d of AB system, *J* = 13.4 Hz, 1H, $^{12}CH_2$), 3.44 (d of AB system, *J* = 13.4 Hz, 1H, $^{12}CH_2$), 2.82-2.18 (m, 6H, $^{10}CH_2$, $^{8}CH_2$, $^{7}CH_2$ and $^{6}CH_2$), 2.11-1.89 (m, 2H, $^{11}CH_2$), 1.74-1.54 (m, 2H, ^{7a}CH and $^{7}CH_2$), 0.93-0.72 (m, 2H, $^{14\text{ or }15}CH_2$ and ^{13}CH), 0.66-0.41 (m, 2H, $^{14\text{ or }15}CH_2$), 0.30-0.17 (m, 1H, $^{14\text{ or }15}CH_2$) ppm. **^{13}C NMR** (75 MHz, $CDCl_3$): δ 169.4 (^{5}CO), 138.9 (^{Ar}Cq), 128.8, 128.4, 127.1 (^{Ar}CH), 92.6 (^{11a}Cq), 68.0 ($^{2}CH_2$), 62.6 ($^{12}CH_2$), 59.9 (^{3}CH), 54.9 ($^{8}CH_2$), 50.8 ($^{10}CH_2$), 40.4 (^{7a}CH), 31.8 ($^{11}CH_2$), 31.1 ($^{6}CH_2$), 22.5 ($^{7}CH_2$), 15.8 (^{13}CH), 4.6 ($^{14\text{ or }15}CH_2$), 2.7 ($^{14\text{ or }15}CH_2$) ppm. **HRMS (ESI, m/z)**: $[M+H]^+$ calcd. for $C_{20}H_{27}N_2O_2$, 327.2071; found: 327.2073.

(3S,7aR,11aR)-9-benzyl-3-tert-butyl-2,3,6,7,7a,8,10,11-octahydrooxazolo[2,3-j][1,6]naphthyridin-5-one **(7)**. The product **7** was obtained from (2S)-2-amino-3,3-dimethyl-butan-1-ol using general protocol 1. The crude was purified by preparative HPLC using H_2O + 0.1% HCOOH/MeCN + 0.1% HCOOH (90/10 to 0/100) to afford the desired product **7** (Yield = 40%, yellow oil), as a single diastereoisomer. **^{1}H NMR** (300 MHz, CD_2Cl_2): δ 7.36-7.19 (m, 5H, ^{Ar}CH), 4.11 (t, *J* = 6.9 Hz, 1H, ^{3}CH),

3.85 (d, *J* = 6.5 Hz, 2H, $^{2}CH_2$), 3.53 (d, *J* = 13.3 Hz, 1H, $^{12}CH_2$), 3.41 (d, *J* = 13.3 Hz, 1H, $^{12}CH_2$), 2.77-2.69 (m, 1H, $^{10}CH_2$), 2.61-2.57 (m, 1H, $^{8}CH_2$), 2.58-2.49 (m, 1H, $^{6}CH_2$), 2.45-2.27 (m, 3H, $^{8}CH_2$, $^{7}CH_2$, and $^{6}CH_2$), 2.20 (dt, *J* = 12.0 Hz, *J* = 3.4 Hz, 1H, $^{10}CH_2$), 1.98 (dt, *J* = 13.3 Hz, *J* = 4.7 Hz, 1H, $^{11}CH_2$), 1.90-1.82 (m, 1H, $^{11}CH_2$), 1.73-1.52 (m, 2H, $^{7}CH_2$ and ^{7a}CH), 0.92 (s, 9H, $^{14}CH_3$, $^{15}CH_3$ and $^{16}CH_3$) ppm. **^{13}C NMR** (75 MHz, CD_2Cl_2): δ 172.7 (^{5}CO), 139.5 (^{Ar}Cq), 129.1, 128.5, 127.2 (^{Ar}CH), 94.3 (^{11a}Cq), 64.8 (^{3}CH), 64.5 ($^{2}CH_2$), 62.7 ($^{12}CH_2$), 54.9 ($^{8}CH_2$), 50.9 ($^{10}CH_2$), 40.2 (^{7a}CH), 34.8 (^{13}Cq), 32.7 ($^{11}CH_2$), 31.0 ($^{6}CH_2$), 27.8 ($^{14}CH_3$, $^{15}CH_3$ and $^{16}CH_3$), 20.9 ($^{7}CH_2$) ppm. **HRMS (ESI, m/z)**: $[M+H]^+$ calcd. for $C_{21}H_{31}N_2O_2$, 343.2386; found: 343.2394.

*(3S,7aR,11aR)-3-isopropyl-3,6,7,7a,8,9,10,11-octahydro-2H-oxazolo[2,3-j][1,6]naphthyridin-5-one;formic acid **(14)**.* Compound **1** (655 mg, 1.99 mmol, 1 eq) was dissolved in methanol (20 mL), then were added Pd/C 10% (127 mg, 1.20 mmol, 0.12 mmol, 10 mol%) and ammonium formate (629 mg, 9.97 mmol, 5 eq). The mixture was refluxed during 30 minutes. The solution was filtered over celite, then the filtrate was concentrated under reduced pressure to afford the desired product **14** with a quantitative yield as a white powder. **^{1}H NMR** (300 MHz, CD_2Cl_2) : δ 8.44 (brs, 1H), 4.13-3.99 (m, 2H), 3.77 (dd, *J* = 8.3, 5.6 Hz, 1H), 3.35-3.11 (m, 3H), 2.99 (td, *J* = 13.1, 3.2 Hz, 1H), 2.68-2.55 (m, 1H), 2.48-2.20 (m, 2H), 2.10 (td, *J* = 14.4, 4.6 Hz, 1H), 2.01-1.70 (m, 4H), 0.92 (d, *J* = 6.4 Hz, 3H), 0.90 (d, *J* = 6.4 Hz, 3H) ppm. **HRMS (ESI, m/z)**: $[M+H]^+$ calcd. for $C_{13}H_{22}N_2O_2$, 239.1760; found 239.1759.

General protocol 2: Alkylation of compound 14

Compound **14** (1 eq) was dissolved in MeCN (0.1N), then K_2CO_3(3 eq) and the appropriate bromide (1-1.5 eq), and NaI (0-1 eq) were added. The solution was stirred at room temperature. When the conversion of **14** into the desired product was judged complete by LC/MS or TLC, the solvent was removed under reduced pressure. The residue obtained was dissolved in H_2O and extracted with dichloromethane. The organic layer was dried over $MgSO_4$, filtered and concentrated under vacuum to give the crude product, which was purified by flash chromatography column over silica gel using cyclohexane/ethyl acetate (1/0 to 0/1) to afford the corresponding desired lactams.

(3S,7aR,11aR)-3-isopropyl-9-(p-tolylmethyl)-2,3,6,7,7a,8,10,11-octahydrooxazolo[2,3-j][1,6]naphthyridin-5-one **(9)**.The product **9** was obtained from 1-(bromomethyl)-4-methyl-benzene using general protocol 2 (Yield = 28%), as a white powder. **^{1}H NMR** (300 MHz, $CDCl_3$): δ 7.19 (d of AB system, *J* = 8.0 Hz, 2H, ^{Ar}CH), 7.11 (d of AB system, *J* = 8.0 Hz, 2H, ^{Ar}CH), 4.12-4.04 (m, 1H, ^{3}CH), 3.97 (dd, *J* = 8.6, 7.6 Hz, 1H, $^{2}CH_2$), 3.76 (dd, *J* = 8.6, 6.2 Hz, 1H, $^{2}CH_2$), 3.50 (d of AB system, *J* = 13.1 Hz, 1H, $^{12}CH_2$), 3.36 (d of AB system, *J* = 13.1 Hz, 1H, $^{12}CH_2$), 2.77-2.62 (m, 2H, $^{10}CH_2$, and $^{8}CH_2$), 2.62-2.50 (m, 1H, $^{6}CH_2$), 2.46-2.34 (m,3H, $^{8}CH_2$, $^{7}CH_2$, and $^{6}CH_2$), 2.30 (s, 3H, $^{16}CH_3$), 2.24-2.13 (m, 1H, $^{10}CH_2$), 2.07-1.88 (m, 2H, ^{13}CH, and $^{11}CH_2$), 1.84-1.71 (m, 1H, $^{11}CH_2$), 1.70-1.54 (m, 2H, ^{7a}CH, and $^{7}CH_2$), 0.94 (d, *J* =

6.8 Hz, 3H, $^{14\text{ or }15}CH_3$), 0.89 (d, *J* = 6.8 Hz, 3H, $^{14\text{ or }15}CH_3$) ppm. **^{13}C NMR** (75 MHz, $CDCl_3$): δ 170.3 (^{5}CO), 136.7, 135.9 (^{Ar}Cq), 129.0, 128.7 (^{Ar}CH), 92.8 (^{11a}Cq), 66.2 ($^{2}CH_2$), 62.3 ($^{12}CH_2$), 61.3 (^{3}CH), 54.8 ($^{8}CH_2$), 50.7 ($^{10}CH_2$), 40.5 (^{7a}CH), 32.5 (^{13}CH), 32.4 ($^{11}CH_2$), 30.9 ($^{6}CH_2$), 22.0 ($^{7}CH_2$), 21.2 ($^{16}CH_3$), 19.9 ($^{14\text{ or }15}CH_3$), 18.7 ($^{14\text{ or }15}CH_3$) ppm. **HRMS (ESI,m/z)**: $[M+H]^+$ calcd. for $C_{21}H_{30}N_2O_2$, 343.2386; found 343.2398.

(3S,7aR,11aR)-3-isopropyl-9-[(4-methoxyphenyl)methyl]-2,3,6,7,7a,8,10,11-octahydrooxazolo[2,3-j][1,6]naphthyridin-5-one **(10)**. The product **10** was obtained from 1-(bromomethyl)-4-methoxy-benzene using general protocol 2 (Yield = 45%), as a colorless oil. **^{1}H NMR** (300 MHz, $CDCl_3$): δ 7.21 (d of AB system, *J* = 8.6 Hz, 2H, ^{Ar}CH), 6.85 (d of AB system, *J* = 8.6 Hz, 2H, ^{Ar}CH), 4.14-4.03 (m, 1H, ^{3}CH), 3.98 (dd, *J* = 8.6, 7.6 Hz, 1H, $^{2}CH_2$), 3.80 (s, 3H, $^{16}CH_3$), 3.79-3.73 (m, 1H, $^{2}CH_2$), 3.48 (d of AB system, *J* = 13.0 Hz, 1H, $^{12}CH_2$), 3.34 (d of AB system, *J* = 13.0 Hz, 1H, $^{12}CH_2$), 2.76-2.63 (m, 2H, $^{10}CH_2$, and $^{8}CH_2$), 2.61-2.51 (m, 1H, $^{6}CH_2$), 2.45-2.28 (m, 3H, $^{8}CH_2$, $^{7}CH_2$ and $^{6}CH_2$), 2.24-2.13 (m, 1H, $^{10}CH_2$), 2.07-1.89 (m, 2H, ^{13}CH and $^{11}CH_2$), 1.82-1.71 (m, 1H, $^{11}CH_2$), 1.70-1.54 (m, 2H, ^{7a}CH and $^{7}CH_2$), 0.94 (d, *J* = 6.9 Hz, 3H, $^{14\text{ or }15}CH_3$), 0.90 (d, *J* = 6.8 Hz, 3H, $^{14\text{ or }15}CH_3$) ppm. **^{13}C NMR** (75 MHz, $CDCl_3$): δ 170.3 (^{5}CO), 158.8, 130.9 (^{Ar}Cq), 129.9, 113.7 (^{Ar}CH), 92.8 (^{11a}Cq), 66.2 ($^{2}CH_2$), 61.9 ($^{12}CH_2$), 61.3 (^{3}CH), 55.4 ($^{16}CH_3$), 54.7 ($^{8}CH_2$), 50.6 ($^{10}CH_2$), 40.4 (^{7a}CH), 32.5 (^{13}CH), 32.4 ($^{11}CH_2$), 30.9 ($^{6}CH_2$), 22.0 ($^{7}CH_2$), 19.9 ($^{14\text{ or }15}CH_3$), 18.7 ($^{14\text{ or }15}CH_3$) ppm. **HRMS (ESI,m/z)**: $[M+H]^+$ calcd. for $C_{21}H_{30}N_2O_3$, 359.2335; found 359.2314.

(3S,7aR,11aR)-9-[(4-chlorophenyl)methyl]-3-isopropyl-2,3,6,7,7a,8,10,11-octahydrooxazolo[2,3-j][1,6]naphthyridin-5-one **(11).** The compound **11** was obtained from 1-chloro-4-(chloromethyl)benzene using general protocol 2 (Yield = 42%), as a colorless oil. **^{1}H NMR** (300 MHz, $CDCl_3$): δ 7.30-7.21 (m, 4H, ^{Ar}CH), 4.14-4.05 (m, 1H, ^{3}CH), 3.98 (dd, *J* = 8.6, 7.6 Hz, 1H, $^{2}CH_2$), 3.76 (dd, *J* = 8.6, 6.2 Hz, 1H, $^{2}CH_2$), 3.49 (d of AB system, *J* = 13.5 Hz, 1H, $^{12}CH_2$), 3.37 (d of AB system, *J* = 13.5 Hz, 1H, $^{12}CH_2$), 2.74-2.61 (m, 2H ; $^{10}CH_2$ and $^{8}CH_2$), 2.60-2.52 (m, 1H, $^{6}CH_2$), 2.50-2.29 (m, 3H, $^{8}CH_2$, $^{7}CH_2$ and $^{6}CH_2$), 2.26-2.15 (m, 1H, $^{10}CH_2$), 2.08-1.89 (m, 2H, ^{13}CH and $^{11}CH_2$), 1.84-1.76 (m, 1H, $^{11}CH_2$), 1.72-1.56 (m, 2H, ^{7a}CH and $^{7}CH_2$), 0.94 (d, *J* = 6.8 Hz, 3H, $^{14\text{ or }15}CH_3$), 0.89 (d, *J* = 6.8 Hz, 3H, $^{14\text{ or }15}CH_3$) ppm. **^{13}C NMR** (75 MHz, $CDCl_3$): δ 170.2 (^{5}CO), 137.5, 132.7 (^{Ar}Cq), 130.0, 128.5 (^{Ar}CH), 92.6 (^{11a}Cq), 66.2 ($^{2}CH_2$), 61.8 ($^{12}CH_2$), 61.3 (^{3}CH), 54.8 ($^{8}CH_2$), 50.7 ($^{10}CH_2$), 40.4 (^{7a}CH), 32.4 (^{13}CH), 32.4 ($^{11}CH_2$), 30.8 ($^{6}CH_2$), 22.0 ($^{7}CH_2$), 19.9 ($^{14\text{ or }15}CH_3$), 18.7 ($^{14\text{ or }15}CH_3$) ppm. **HRMS (ESI, m/z)**: $[M+H]^+$ calcd. for $C_{20}H_{28}N_2O_2Cl$, 363.1839; found 363.1872.

(3S,7aR,11aR)-3-isopropyl-9-[[4-(trifluoromethyl)phenyl]methyl]-2,3,6,7,7a,8,10,11-octahydrooxazolo[2,3-j][1,6]naphthyridin-5-one **(12)**. The product **12** was obtained from 1-(bromomethyl)-4-(trifluoromethyl)benzene using general protocol 2 (Yield = 73%), as a white powder. **^{1}H NMR** (300 MHz, CD_2Cl_2) : δ 7.57 (d of AB system, *J* = 8.1 Hz, 2H, ^{Ar}CH), 7.47 (d of AB system, *J* = 8.1 Hz, 2H, ^{Ar}CH), 4.07-3.94 (m, 2H, ^{3}CH and $^{2}CH_2$), 3.75 (dd, *J* = 8.0, 5.7 Hz, 1H, $^{2}CH_2$), 3.58 (d of AB system,

J = 13.9 Hz, 1H, $^{12}CH_2$), 3.48 (d of AB system, *J* = 13.9 Hz, 1H, $^{12}CH_2$), 2.73-2.61 (m, 2H, $^{10}CH_2$ and $^{8}CH_2$), 2.57-2.45 (m, 2H, $^{8}CH_2$ and $^{6}CH_2$), 2.41-2.28 (m, 2H, $^{7}CH_2$ and $^{6}CH_2$), 2.27-2.18 (m, 1H, $^{10}CH_2$), 2.03-1.90 (m, 2H, ^{13}CH and $^{11}CH_2$), 1.82-1.74 (m, 1H, $^{11}CH_2$), 1.69-1.56 (m, 2H, ^{7a}CH and $^{7}CH_2$), 0.91 (d, *J* = 6.8 Hz, 3H, $^{14\text{ or }15}CH_3$), 0.88 (d, *J* = 6.8 Hz, 3H, $^{14\text{ or }15}CH_3$) ppm. **^{13}C NMR** (75 MHz, CD_2Cl_2): δ 170.0 (^{5}CO), 144.0 (^{Ar}Cq), 129.2 (q, *J* = 32.2 Hz, ^{Ar}Cq), 129.2 (^{Ar}CH), 125.4 (q, *J* = 3.7 Hz, ^{Ar}CH), 124.8 (q, *J* = 272.1 Hz, ^{CF3}Cq), 92.7 (^{11a}Cq), 66.4($^{2}CH_2$), 62.2 ($^{12}CH_2$), 61.5 (^{3}CH), 55.3 ($^{8}CH_2$), 51.0 ($^{10}CH_2$), 40.8 (^{7a}CH), 32.8 (^{13}CH), 32.6 ($^{11}CH_2$), 31.2 ($^{6}CH_2$), 32.3 ($^{7}CH_2$), 19.9 ($^{14\text{ or }15}CH_3$), 18.7 ($^{14\text{ or }15}CH_3$) ppm. **LCMS (ESI, m/z)**: Tr = 2.83 min, $[M+H]^+$ = 397. **HRMS (ESI, m/z)**: $[M+H]^+$ calcd. for $C_{21}H_{27}N_2O_2F_3$, 397.2103; found 396.2101.

(3S,7aR,11aR)-3-isopropyl-9-[[4-(trifluoromethoxy)phenyl]methyl]-2,3,6,7,7a,8,10,11-octahydrooxazolo[2,3-j][1,6]naphthyridin-5-one **(13).** The product **13** was obtained from 1-(bromomethyl)-4-(trifluoromethoxy)benzene using general protocol 2 (Yield = 77%), as a colorless oil. **^{1}H NMR** (300 MHz, CD_2Cl_2) : δ 7.38 (d of AB system, *J* = 8.6 Hz, 2H, ^{Ar}CH), 7.17 (d of AB system, *J* = 8.6 Hz, 2H, ^{Ar}CH), 4.07-3.94 (m, 2H, ^{3}CH and $^{2}CH_2$), 3.75 (dd, *J* = 8.0, 5.7 Hz, 1H, $^{2}CH_2$), 3.52 (d of AB system, *J* = 13.6 Hz, 1H, $^{12}CH_2$), 3.42 (d of AB system, *J* = 13.6 Hz, 1H, $^{12}CH_2$), 2.74-2.60 (m, 2H, $^{10}CH_2$ and $^{8}CH_2$), 2.58-2.42 (m, 2H, $^{8}CH_2$ and $^{6}CH_2$), 2.40-2.26 (m, 2H, $^{7}CH_2$ and $^{6}CH_2$), 2.26-2.14 (m, 1H, $^{10}CH_2$), 2.04-1.87 (m, 2H, ^{13}CH and $^{11}CH_2$), 1.83-1.74 (m, 1H, $^{11}CH_2$), 1.72-1.54 (m, 2H, ^{7a}CH, and $^{7}CH_2$), 0.91 (d, *J* = 6.7 Hz, 3H, $^{14\text{ or }15}CH_3$), 0.88 (d, *J* = 6.7 Hz, 3H, $^{14\text{ or }15}CH_3$) ppm. **^{13}C NMR** (75 MHz, CD_2Cl_2): δ 170.0 (^{5}CO), 148.5, 138.6 (^{Ar}Cq), 130.3, 121.1 (^{Ar}CH), 120.7 (q, *J* = 250.1 Hz, ^{CF3}Cq), 92.8 (^{11a}Cq), 66.4($^{2}CH_2$), 61.9 ($^{12}CH_2$), 61.6 (^{3}CH), 55.3 ($^{8}CH_2$), 50.9 ($^{10}CH_2$), 40.8 (^{7a}CH), 32.8 (^{13}CH), 32.7 ($^{11}CH_2$), 31.2 ($^{6}CH_2$), 32.3 ($^{7}CH_2$), 20.0 ($^{14\text{ or }15}CH_3$), 18.8 ($^{14\text{ or }15}CH_3$) ppm. **LCMS (ESI, m/z)**: Tr = 2.82 min, $[M+H]^+$ = 413. **HRMS (ESI, m/z)**: $[M+H]^+$ calcd. for $C_{21}H_{28}N_2O_3F_3$, 413.2052; found 413.2056.

(3S,7aR,11aR)-3-isopropyl-9-[[6-(trifluoromethyl)-3-pyridyl]methyl]-2,3,6,7,7a,8,10,11-octahydrooxazolo[2,3-j][1,6]naphthyridin-5-one **(13).** To a solution of compound **14** (500 mg, 1.76 mmol, 1 eq) in dichloroethane (4 mL), were added 6-(trifluoromethyl)pyridine-3-carbaldehyde (1.1 g, 6.29 mmol, 3.6 eq), titanium isopropoxide (937 µL, 3.15 mmol, 1.8 eq), $NaBH(OAc)_3$ (1.33 g, 6.29 mmol, 3.6 eq). The mixture was stirred at room temperature overnight. The solvent was removed under vacuum, the mixture was then taken up in CH_2Cl_2 and washed with a saturated aqueous solution of Na_2CO_3. The organic layer was dried over magnesium sulfate, filtered and concentrated under vacuum. The product was purified by flash chromatography column over silica gel using cyclohexane/ethyl acetate (1/0 to 0/1) to afford the desired product **13** (493 mg, 71%) as a white powder. **^{1}H NMR** (300 MHz, $CDCl_3$): δ 8.66 (brs, 1H, ^{Ar}CH), 7.85 (dd, *J* = 8.0, 1.3 Hz, 1H, ^{Ar}CH), 7.64 (d, *J* = 8.0 Hz, 1H, ^{Ar}CH), 4.14-4.06 (m, 1H, ^{3}CH), 3.99 (dd, *J* = 8.5, 8.0 Hz, 1H, $^{2}CH_2$), 3.78 (dd, *J* = 8.5, 6.2 Hz, 1H, $^{2}CH_2$), 3.62 (d of AB system, *J* = 14.1 Hz, 1H, $^{12}CH_2$), 3.52 (d of AB system, *J* = 14.1 Hz, 1H, $^{12}CH_2$), 2.75-2.52 (m, 4H, $^{10}CH_2$, $^{8}CH_2$ and $^{6}CH_2$), 2.48-2.25 (m, 3H, $^{10}CH_2$, $^{7}CH_2$ and $^{6}CH_2$), 2.07-1.91 (m,

2H, ^{13}CH and ^{11}CH$_2$), 1.85-1.77 (m, 1H, ^{11}CH$_2$), 1.75-1.59 (m, 2H, ^{7a}CH and ^{7}CH$_2$), 0.95 (d, *J* = 6.8 Hz, 3H, $^{14\text{ or }15}$CH$_3$), 0.91 (d, *J* = 6.8 Hz, 3H, $^{14\text{ or }15}$CH$_3$) ppm. **^{13}C NMR** (75 MHz, $CDCl_3$): δ 170.1 (^{5}CO), 129.2 (^{Ar}CH), 147.2 (q, *J* = 33.5 Hz, ^{Ar}Cq), 137.9 (^{Ar}Cq), 137.5 (^{Ar}CH), 121.5 (q, *J* = 272.0 Hz, ^{CF3}Cq), 120.3 (q, *J* = 3.7 Hz, ^{Ar}CH), 92.3 (^{11a}Cq), 66.3 (^{2}CH$_2$), 61.3 (^{12}CH$_2$), 59.4 (^{3}CH), 55.0 (^{8}CH$_2$), 50.8 (^{10}CH$_2$), 40.3 (^{7a}CH), 32.4 (^{13}CH), 32.3 (^{11}CH$_2$), 30.7 (^{6}CH$_2$), 21.9 (^{7}CH$_2$), 19.9, 18.7 ($^{14\text{ and }15}$CH$_3$) ppm. **LCMS (ESI, m/z)**: Tr = 2.77 min, $[M+H]^+$ = 398. **HRMS (ESI, m/z)**: $[M+H]^+$ calcd. for $C_{20}H_{27}N_3O_2F_3$, 398.2055; found 398.2044.

ASSOCIATED CONTENT

Supporting information

The Supporting Information is available free of charge at...

All biological, ADME and X-ray diffraction methods are detailed. Supplementary tables and figures are shown. ^{1}H and ^{13}C NMR spectra, HRMS spectra of all synthesized compounds as well as 2-D NMR and HPLC-MS traces for lead compounds are provided (PDF)

Compound SMILES and biological data (CSV)

Data availability

Atomic coordinates and structure factors reported in this paper (crystal structure of **BDM44410, 1**) have been deposited in the Cambridge Structural Database under accession number CCDC 2143694. Whole genome sequencing data (fastq files) for parental and **BDM44410 (1)** resistant H37Rv isolates (RC14.2, RC28.1) have been deposited at NCBI (BioProject ID: PRJNA808942)

AUTHOR INFORMATION

Corresponding authors

Ruben C. Hartkoorn (ruben.hartkoorn@inserm.fr)

Baptiste Villemagne (baptiste.villemagne@univ-lille.fr)

Nicolas Willand (nicolas.willand@univ-lille.fr)

Author contributions

SD, ST, CH, TA, LF, LK, NW, BV, and RCH designed experiments. NW and BD designed, generated and compiled the screened chemical library. ST, TA, LF MF, BD, NW and BV designed, synthesised and characterized TriSLa analogues. AH, FL, NW and RCH performed the chemical library screening. Selection of TriSLa resistant isolates was performed by SD and RCH. Metabolic stability was determined by CP, ME and BV. Phys-chem properties were determined by CP, ME, and BV. Anti-bacterial *In vitro* profiling of TriSLa compounds was performed by SD and RCH. Biochemical validation

was performed by SD, PC and RCH. *In vivo* efficacy studies on *M. marinum* infected zebrafish and analysis were performed by CH and LK. SD, ST, CH, LF, MF, BD, LK, NW, BV, and RCH wrote the paper. NW, BV and RCH obtained funding for this work.

Competing interests

SD, ST, TA, LF, MF, BD, NW, BV and RCH, are inventors on patent application covering the TriSLa described in this manuscript. The remaining authors declare no competing interests.

Acknowledgements:

We thank F. Capet and P. Roussel from the X-ray platform of Chevreul Institute (FR CNRS 2638), for supporting data collection and solving the x-ray crystal structure. We thank V. Landry (U1177- Drugs and Molecules for Living Systems) for cytotoxicity experiments. We thank BLS-3 Facility staff (N. Vandenabeele, R. Prath and S. Marin) at the Institut Pasteur de Lille for technical support. We thank E. Anoz Carbonell for unbiased MIC analysis. We are grateful to P. Richard and M. Plays for zebrafish husbandry.

This research was financially co-funded by NL4Tb, Atip-Avenir, SMARt-Lab and CPER grants. The NL4Tb grant was funded by the French National Research Agency (ANR-19-CE18-0034-01). The SMARt-Lab grant was funded by European Union under the European Regional Development Fund (ERDF), by the Hauts De France Regional Council (Contract n°NP0020070) and by I-Site ULNE (ANR-16-IDEX-0004 ULNE). The CPER grants were funded by European Union under the European Regional Development Fund (ERDF) and by the Hauts de France regional Council (contract n°20002842 and contract n° 18006176), the MEL (contract n°2017_ESR_14 and contract_2020_ESR_06), and the French State (contract n° 2018-R3-CTRL-Phase2 and contract n°2020-R3-CTRL_IPL_Phase4). The compound management and physicochemical/ADME properties measurement were supported by ChemBioFrance through the ARIADNE platform (Lille, France).

ABBREVIATIONS

BDQ, bedaquiline; cfu, colony forming unit; dpi, days post-infection; FPC, fluorescent pixel count; hpf, hours post-fertilization; INH, isoniazid; MBP, maltose-binding protein; MDR, multi-drug resistant; *Mtb*, *Mycobacterium tuberculosis*; REMA, resazurin microtiter assay; RIF, rifampicin; XDR, extensively drug resistant.

References

(1) World Health Organization. *Global Tuberculosis Report 2021*; Geneva, 2021.

(2) Connolly, L. E.; Edelstein, P. H.; Ramakrishnan, L. Why Is Long-Term Therapy Required to Cure Tuberculosis? *PLoS Med.* **2007**, *4* (3), e120. https://doi.org/10.1371/journal.pmed.0040120.

(3) World Health Organization. *Global Tuberculosis Report 2020*; Geneva, 2020.

(4) World Health Organization. *Global Priority List Of Antibiotic-Resistant Bacteria To Guide Research, Discovery And Development Of New Antibiotics*; 2017. https://doi.org/10.1016/S1473-3099(09)70222-1.

(5) Palomino, J. C.; Martin, A. TMC207 Becomes Bedaquiline, a New Anti-TB Drug. *Future Microbiol.* **2013**, *8* (9), 1071–1080. https://doi.org/10.2217/fmb.13.85.

(6) Ryan, N. J.; Lo, J. H. Delamanid: First Global Approval. *Drugs* **2014**, *74* (9), 1041–1045. https://doi.org/10.1007/s40265-014-0241-5.

(7) Keam, S. J. Pretomanid: First Approval. *Drugs* **2019**, *79* (16), 1797–1803. https://doi.org/10.1007/s40265-019-01207-9.

(8) Tiberi, S.; du Plessis, N.; Walzl, G.; Vjecha, M. J.; Rao, M.; Ntoumi, F.; Mfinanga, S.; Kapata, N.; Mwaba, P.; McHugh, T. D.; Ippolito, G.; Migliori, G. B.; Maeurer, M. J.; Zumla, A. Tuberculosis: Progress and Advances in Development of New Drugs, Treatment Regimens, and Host-Directed Therapies. *Lancet Infect. Dis.* **2018**, *18* (7), e183–e198. https://doi.org/10.1016/S1473-3099(18)30110-5.

(9) Tornheim, J. A.; Dooley, K. E. The Global Landscape of Tuberculosis Therapeutics. *Annu. Rev. Med.* **2019**, *70* (October 2018), 105–120. https://doi.org/10.1146/annurev-med-040717-051150.

(10) J Libardo, M. D.; Boshoff, H. I.; Barry, C. E. The Present State of the Tuberculosis Drug Development Pipeline. *Curr. Opin. Pharmacol.* **2018**, *42*, 81–94. https://doi.org/10.1016/j.coph.2018.08.001.

(11) Mikušová, K.; Ekins, S. Learning from the Past for TB Drug Discovery in the Future. *Drug Discov. Today* **2017**, *22* (3), 534–545. https://doi.org/10.1016/j.drudis.2016.09.025.

(12) Ballell, L.; Bates, R. H.; Young, R. J.; Alvarez-Gomez, D.; Alvarez-Ruiz, E.; Barroso, V.; Blanco, D.; Crespo, B.; Escribano, J.; González, R.; Lozano, S.; Huss, S.; Santos-Villarejo, A.; Martín-Plaza, J. J.; Mendoza, A.; Rebollo-Lopez, M. J.; Remuiñan-Blanco, M.; Lavandera, J. L.; Pérez-Herran, E.; Gamo-Benito, F. J.; García-Bustos, J. F.; Barros, D.; Castro, J. P.; Cammack, N. Fueling Open-Source Drug Discovery: 177 Small-Molecule Leads against Tuberculosis. *ChemMedChem* **2013**, *8* (2), 313–321. https://doi.org/10.1002/cmdc.201200428.

(13) Kumar, A.; Zhang, K. Y. J. Advances in the Development of Shape Similarity Methods and Their Application in Drug Discovery. *Front. Chem.* **2018**, *6* (JUL), 1–21. https://doi.org/10.3389/fchem.2018.00315.

(14) Deprez-Poulain, R.; Willand, N.; Boutillon, C.; Nowogrocki, G.; Azaroual, N.; Deprez, B. A Simple Reaction to Produce Small Structurally Complex and Diverse Molecules. *Tetrahedron Lett.* **2004**, *45* (27), 5287–5290. https://doi.org/10.1016/j.tetlet.2004.05.008.

(15) Willand, N.; Beghyn, T.; Nowogrocki, G.; Gesquiere, J.-C.; Deprez, B. Synthesis and Structural Studies of a Novel Scaffold for Drug Discovery: A 4,5-Dihydro-3H-Spiro[1,5-Benzoxazepine-2,4'-Piperidine]. *Tetrahedron Lett.* **2004**, *45* (5), 1051–1054.

https://doi.org/10.1016/j.tetlet.2003.11.079.

(16) Willand, N.; Folléas, B.; Boutillon, C.; Verbraeken, L.; Gesquière, J.-C.; Tartar, A.; Deprez, B. Efficient, Two-Step Synthesis of N-Substituted Nortropinone Derivatives. *Tetrahedron Lett.* **2007**, *48* (29), 5007–5011. https://doi.org/10.1016/j.tetlet.2007.05.110.

(17) Malaquin, S.; Jida, M.; Courtin, J.; Laconde, G.; Willand, N.; Deprez, B.; Deprez-Poulain, R. Water-Based Conditions for the Microscale Parallel Synthesis of Bicyclic Lactams. *Tetrahedron Lett.* **2013**, *54* (6), 562–567. https://doi.org/10.1016/j.tetlet.2012.11.082.

(18) Tran, N. C.; Dhondt, H.; Flipo, M.; Deprez, B.; Willand, N. Synthesis of Functionalized 2-Isoxazolines as Three-Dimensional Fragments for Fragment-Based Drug Discovery. *Tetrahedron Lett.* **2015**, *56* (27), 4119–4123. https://doi.org/10.1016/j.tetlet.2015.05.035.

(19) Prevet, H.; Flipo, M.; Roussel, P.; Deprez, B.; Willand, N. Microwave-Assisted Synthesis of Functionalized Spirohydantoins as 3-D Privileged Fragments for Scouting the Chemical Space. *Tetrahedron Lett.* **2016**, *57* (26), 2888–2894. https://doi.org/10.1016/j.tetlet.2016.05.065.

(20) Blondiaux, N.; Moune, M.; Desroses, M.; Frita, R.; Flipo, M.; Mathys, V.; Soetaert, K.; Kiass, M.; Delorme, V.; Djaout, K.; Trebosc, V.; Kemmer, C.; Wintjens, R.; Wohlkönig, A.; Antoine, R.; Huot, L.; Hot, D.; Coscolla, M.; Feldmann, J.; Gagneux, S.; Locht, C.; Brodin, P.; Gitzinger, M.; Déprez, B.; Willand, N.; Baulard, A. R. Reversion of Antibiotic Resistance in Mycobacterium Tuberculosis by Spiroisoxazoline SMARt-420. *Science (80-.).* **2017**, *355* (6330), 1206–1211. https://doi.org/10.1126/science.aag1006.

(21) Prevet, H.; Moune, M.; Tanina, A.; Kemmer, C.; Herledan, A.; Frita, R.; Wohlkönig, A.; Bourotte, M.; Villemagne, B.; Leroux, F.; Gitzinger, M.; Baulard, A. R.; Déprez, B.; Wintjens, R.; Willand, N.; Flipo, M. A Fragment-Based Approach towards the Discovery of N-Substituted Tropinones as Inhibitors of Mycobacterium Tuberculosis Transcriptional Regulator EthR2. *Eur. J. Med. Chem.* **2019**, *167*, 426–438. https://doi.org/10.1016/j.ejmech.2019.02.023.

(22) von Korff, M.; Sander, T. About Complexity and Self-Similarity of Chemical Structures in Drug Discovery. In *Chaos and Complex Systems*; Springer Berlin Heidelberg: Berlin, Heidelberg, 2013; pp 301–306. https://doi.org/10.1007/978-3-642-33914-1_39.

(23) Sander, T.; Freyss, J.; von Korff, M.; Rufener, C. DataWarrior: An Open-Source Program For Chemistry Aware Data Visualization And Analysis. *J. Chem. Inf. Model.* **2015**, *55* (2), 460–473. https://doi.org/10.1021/ci500588j.

(24) Koul, A.; Vranckx, L.; Dhar, N.; Göhlmann, H. W. H.; Özdemir, E.; Neefs, J.-M.; Schulz, M.; Lu, P.; Mørtz, E.; McKinney, J. D.; Andries, K.; Bald, D. Delayed Bactericidal Response of Mycobacterium Tuberculosis to Bedaquiline Involves Remodelling of Bacterial Metabolism. *Nat. Commun.* **2014**, *5* (1), 3369. https://doi.org/10.1038/ncomms4369.

(25) Vocat, A.; Hartkoorn, R. C.; Lechartier, B.; Zhang, M.; Dhar, N.; Cole, S. T.; Sala, C. Bioluminescence for Assessing Drug Potency against Nonreplicating Mycobacterium Tuberculosis. *Antimicrob. Agents Chemother.* **2015**, *59* (7), 4012–4019. https://doi.org/10.1128/AAC.00528-15.

(26) Zhang, M.; Sala, C.; Hartkoorn, R. C.; Dhar, N.; Mendoza-Losana, A.; Cole, S. T. Streptomycin-Starved Mycobacterium Tuberculosis 18b, a Drug Discovery Tool for Latent Tuberculosis. *Antimicrob. Agents Chemother.* **2012**, *56* (11), 5782–5789. https://doi.org/10.1128/AAC.01125-12.

(27) Varadi, M.; Anyango, S.; Deshpande, M.; Nair, S.; Natassia, C.; Yordanova, G.; Yuan, D.; Stroe, O.; Wood, G.; Laydon, A.; Žídek, A.; Green, T.; Tunyasuvunakool, K.; Petersen, S.; Jumper, J.;

Clancy, E.; Green, R.; Vora, A.; Lutfi, M.; Figurnov, M.; Cowie, A.; Hobbs, N.; Kohli, P.; Kleywegt, G.; Birney, E.; Hassabis, D.; Velankar, S. AlphaFold Protein Structure Database: Massively Expanding the Structural Coverage of Protein-Sequence Space with High-Accuracy Models. *Nucleic Acids Res.* **2021**, 1–6. https://doi.org/10.1093/nar/gkab1061.

(28) Jumper, J.; Evans, R.; Pritzel, A.; Green, T.; Figurnov, M.; Ronneberger, O.; Tunyasuvunakool, K.; Bates, R.; Žídek, A.; Potapenko, A.; Bridgland, A.; Meyer, C.; Kohl, S. A. A.; Ballard, A. J.; Cowie, A.; Romera-Paredes, B.; Nikolov, S.; Jain, R.; Adler, J.; Back, T.; Petersen, S.; Reiman, D.; Clancy, E.; Zielinski, M.; Steinegger, M.; Pacholska, M.; Berghammer, T.; Bodenstein, S.; Silver, D.; Vinyals, O.; Senior, A. W.; Kavukcuoglu, K.; Kohli, P.; Hassabis, D. Highly Accurate Protein Structure Prediction with AlphaFold. *Nature* **2021**, *596* (7873), 583–589. https://doi.org/10.1038/s41586-021-03819-2.

(29) Murugesan, D.; Ray, P. C.; Bayliss, T.; Prosser, G. A.; Harrison, J. R.; Green, K.; Soares de Melo, C.; Feng, T.-S.; Street, L. J.; Chibale, K.; Warner, D. F.; Mizrahi, V.; Epemolu, O.; Scullion, P.; Ellis, L.; Riley, J.; Shishikura, Y.; Ferguson, L.; Osuna-Cabello, M.; Read, K. D.; Green, S. R.; Lamprecht, D. A.; Finin, P. M.; Steyn, A. J. C.; Ioerger, T. R.; Sacchettini, J.; Rhee, K. Y.; Arora, K.; Barry, C. E.; Wyatt, P. G.; Boshoff, H. I. M. 2-Mercapto-Quinazolinones as Inhibitors of Type II NADH Dehydrogenase and Mycobacterium Tuberculosis : Structure–Activity Relationships, Mechanism of Action and Absorption, Distribution, Metabolism, and Excretion Characterization. *ACS Infect. Dis.* **2018**, *4* (6), 954–969. https://doi.org/10.1021/acsinfecdis.7b00275.

(30) Vilchèze, C.; Weinrick, B.; Leung, L. W.; Jacobs, W. R. Plasticity of Mycobacterium Tuberculosis NADH Dehydrogenases and Their Role in Virulence. *Proc. Natl. Acad. Sci. U. S. A.* **2018**, *115* (7), 1599–1604. https://doi.org/10.1073/pnas.1721545115.

(31) Beites, T.; O'Brien, K.; Tiwari, D.; Engelhart, C. A.; Walters, S.; Andrews, J.; Yang, H.-J.; Sutphen, M. L.; Weiner, D. M.; Dayao, E. K.; Zimmerman, M.; Prideaux, B.; Desai, P. V.; Masquelin, T.; Via, L. E.; Dartois, V.; Boshoff, H. I.; Barry, C. E.; Ehrt, S.; Schnappinger, D. Plasticity of the Mycobacterium Tuberculosis Respiratory Chain and Its Impact on Tuberculosis Drug Development. *Nat. Commun.* **2019**, *10* (1), 4970. https://doi.org/10.1038/s41467-019-12956-2.

(32) Miesel, L.; Weisbrod, T. R.; Marcinkeviciene, J. A.; Bittman, R.; Jacobs, W. R. NADH Dehydrogenase Defects Confer Isoniazid Resistance and Conditional Lethality in Mycobacterium Smegmatis. *J. Bacteriol.* **1998**, *180* (9), 2459–2467. https://doi.org/10.1128/JB.180.9.2459-2467.1998.

(33) Harbut, M. B.; Yang, B.; Liu, R.; Yano, T.; Vilchèze, C.; Cheng, B.; Lockner, J.; Guo, H.; Yu, C.; Franzblau, S. G.; Petrassi, H. M.; Jacobs, W. R.; Rubin, H.; Chatterjee, A. K.; Wang, F. Small Molecules Targeting Mycobacterium Tuberculosis Type II NADH Dehydrogenase Exhibit Antimycobacterial Activity. *Angew. Chemie Int. Ed.* **2018**, *57* (13), 3478–3482. https://doi.org/10.1002/anie.201800260.

(34) Takaki, K.; Cosma, C. L.; Troll, M. A.; Ramakrishnan, L. An In Vivo Platform for Rapid High-Throughput Antitubercular Drug Discovery. *Cell Rep.* **2012**, *2* (1), 175–184. https://doi.org/10.1016/j.celrep.2012.06.008.

(35) Clay, H.; Volkman, H. E.; Ramakrishnan, L. Tumor Necrosis Factor Signaling Mediates Resistance to Mycobacteria by Inhibiting Bacterial Growth and Macrophage Death. *Immunity* **2008**, *29* (2), 283–294. https://doi.org/10.1016/j.immuni.2008.06.011.

(36) Volkman, H. E.; Clay, H.; Beery, D.; Chang, J. C. W.; Sherman, D. R.; Ramakrishnan, L. Tuberculous Granuloma Formation Is Enhanced by a Mycobacterium Virulence Determinant.

PLoS Biol. **2004**, *2* (11), e367. https://doi.org/10.1371/journal.pbio.0020367.

(37) Alibaud, L.; Rombouts, Y.; Trivelli, X.; Burguière, A.; Cirillo, S. L. G.; Cirillo, J. D.; Dubremetz, J.-F.; Guérardel, Y.; Lutfalla, G.; Kremer, L. A Mycobacterium Marinum TesA Mutant Defective for Major Cell Wall-Associated Lipids Is Highly Attenuated in Dictyostelium Discoideum and Zebrafish Embryos. *Mol. Microbiol.* **2011**, *80* (4), 919–934. https://doi.org/10.1111/j.1365-2958.2011.07618.x.

(38) Beghyn, T.; Deprez-Poulain, R.; Willand, N.; Folleas, B.; Deprez, B. Natural Compounds: Leads or Ideas? Bioinspired Molecules for Drug Discovery. *Chem. Biol. Drug Des.* **2008**, *72* (1), 3–15. https://doi.org/10.1111/j.1747-0285.2008.00673.x.

(39) Lee, M.-L.; Schneider, G. Scaffold Architecture and Pharmacophoric Properties of Natural Products and Trade Drugs: Application in the Design of Natural Product-Based Combinatorial Libraries. *J. Comb. Chem.* **2001**, *3* (3), 284–289. https://doi.org/10.1021/cc000097l.

(40) Henkel, T.; Brunne, R. M.; Müller, H.; Reichel, F. Statistical Investigation into the Structural Complementarity of Natural Products and Synthetic Compounds. *Angew. Chemie Int. Ed.* **1999**, *38* (5), 643–647. https://doi.org/10.1002/(SICI)1521-3773(19990301)38:5<643::AID-ANIE643>3.0.CO;2-G.

(41) Hong, W. D.; Gibbons, P. D.; Leung, S. C.; Amewu, R.; Stocks, P. A.; Stachulski, A.; Horta, P.; Cristiano, M. L. S.; Shone, A. E.; Moss, D.; Ardrey, A.; Sharma, R.; Warman, A. J.; Bedingfield, P. T. P.; Fisher, N. E.; Aljayyoussi, G.; Mead, S.; Caws, M.; Berry, N. G.; Ward, S. A.; Biagini, G. A.; O'Neill, P. M.; Nixon, G. L. Rational Design, Synthesis, and Biological Evaluation of Heterocyclic Quinolones Targeting the Respiratory Chain of Mycobacterium Tuberculosis. *J. Med. Chem.* **2017**, *60* (9), 3703–3726. https://doi.org/10.1021/acs.jmedchem.6b01718.

(42) Heikal, A.; Nakatani, Y.; Jiao, W.; Wilson, C.; Rennison, D.; Weimar, M. R.; Parker, E. J.; Brimble, M. A.; Cook, G. M. 'Tethering' Fragment-Based Drug Discovery to Identify Inhibitors of the Essential Respiratory Membrane Protein Type II NADH Dehydrogenase. *Bioorganic Med. Chem. Lett.* **2018**, *28* (13), 2239–2243. https://doi.org/10.1016/j.bmcl.2018.05.048.

(43) Shirude, P. S.; Paul, B.; Roy Choudhury, N.; Kedari, C.; Bandodkar, B.; Ugarkar, B. G. Quinolinyl Pyrimidines: Potent Inhibitors of NDH-2 as a Novel Class of Anti-TB Agents. *ACS Med. Chem. Lett.* **2012**, *3* (9), 736–740. https://doi.org/10.1021/ml300134b.

(44) Lu, L.; Åkerbladh, L.; Ahmad, S.; Konda, V.; Cao, S.; Vocat, A.; Maes, L.; Cole, S. T.; Hughes, D.; Larhed, M.; Brandt, P.; Karlén, A.; Mowbray, S. L. Synthesis and In Vitro Biological Evaluation of Quinolinyl Pyrimidines Targeting Type II NADH-Dehydrogenase (NDH-2). *ACS Infect. Dis.* **2022**, acsinfecdis.1c00413. https://doi.org/10.1021/acsinfecdis.1c00413.

(45) Johansen, M. D.; Kasparian, J. A.; Hortle, E.; Britton, W. J.; Purdie, A. C.; Oehlers, S. H. Mycobacterium Marinum Infection Drives Foam Cell Differentiation in Zebrafish Infection Models. *Dev. Comp. Immunol.* **2018**, *88* (May), 169–172. https://doi.org/10.1016/j.dci.2018.07.022.

Table of Contents Graphic: